Received: 23 November 2021 | Revised: 10 August 2022 | Accepted: 17 August 2022

DOI: 10.1002/eqe.3734

RESEARCH ARTICLE

WILEY

Direct seismic loss estimation of predominantly plan-symmetrical frame buildings using simplified nonlinear models

Aleš Jamšek | **Anže Babič** | **Matjaž Dolšek**

Faculty of Civil and Geodetic Engineering, University of Ljubljana, Ljubljana, Slovenia

Correspondence
Matjaž Dolšek, University of Ljubljana, Ljubljana, SI 1000, Slovenia.
Email: mdolsek@ikpir.fgg.uni-lj.si

Funding information
Slovenian Research Agency, Grant/Award Numbers: P2-0185, Earthquake Engineering

Abstract

The estimation of building seismic risk and loss utilising response history analysis is challenging, especially because the final objective is the seismic loss estimation for building stock. In this paper, this challenge is addressed by developing a simplified nonlinear structural model, which is capable of simulating the seismic response of predominantly plan-symmetrical reinforced concrete frame buildings subjected to ground motions in both horizontal directions. The simplified structural model is plugged into the direct seismic risk and loss estimation methodology. Its capabilities are then demonstrated by estimating the seismic risk and losses for a four-storey office building and a five-storey school building. For the analysed buildings, it is shown that the frequency of collapse, the expected annual loss and the frequency of exceedance of a given loss can be simulated with the same level of accuracy as in the case of the conventional structural model, but with greater numerical robustness and computational efficiency. Research is needed to better define the limitations of the introduced simplified model and extend the capabilities of simplified nonlinear models to more complex structural systems of plan-asymmetrical buildings.

KEYWORDS

IFB model, loss estimation, reinforced concrete frame building, response history analysis, seismic risk assessment, simplified model

1 | INTRODUCTION

Seismic loss estimation provides enhanced information for the evaluation of the seismic performance of new and existing buildings. Several methodologies for seismic loss estimation have been proposed (e.g.[1–7]). However, loss estimation is rarely practised in decision-making related to seismic risk reduction. This can be partly attributed to the limited computational robustness and time-efficiency of the structural models suitable for seismic loss estimation.

The robustness and time-efficiency of a given structural model depend on the analysed building and the modelling approach. In the case of frame buildings, researchers typically utilise conventional multiple-degree-of-freedom (MDOF)

models, in which each beam and column is modelled by at least one finite element (e.g.[8–13]). However, such models are still rarely used for the nonlinear response history analysis of complex building structures due to their limited robustness and time-efficiency. Therefore, simplified structural models have been introduced. One simplified modelling approach anticipates the use of archetype models (e.g.[14,15]). In this approach, which is primarily intended to study the seismic performance of specific building types, idealised MDOF models are defined for archetype configurations that are characteristic of the building type under consideration. Some researchers (e.g.[7,16]) have suggested using a single-degree-of-freedom (SDOF) model developed based on the pushover analysis of a conventional MDOF model. The SDOF models are time-efficient and robust, but they are only capable of estimating the buildings' global response. In order to evaluate the engineering demand parameters (EDPs) at a greater level of detail, for example at the storey level or building component level, the results of the SDOF model must be combined with the results of a pushover analysis utilising the conventional MDOF model.[7]

Another approach to develop a simplified structural model, and one which is not yet practised in loss estimation, is to decrease the number of finite elements in an MDOF model by condensing the degrees of freedom. Such simplified structural models include the generic frame (GF) model and the fish-bone (FB) model.[17–19] Both types of models have undergone several upgrades over the last decade,[11,20–28] making them capable of simulating the seismic response of a large set of different building designs, varying in plan and elevation. In addition, some of these models (e.g.[11,27]) are defined directly based on the building structure input data without utilizing a conventional MDOF model as their reference model, which makes the model definition more straightforward and less time-consuming. However, despite the promising results shown by the GF and FB models, their capability of simulating local EDPs in seismic loss estimation is not yet well understood.

To contribute to the solution of the described challenge, a new simplified structural model is proposed here, and its applicability in loss estimation of predominantly plan-symmetrical frame buildings is analysed. The proposed model, called the improved 3D fish-bone model (IFB3), has been developed based on the previously proposed IFB model, which was validated for low- to mid-rise reinforced concrete frame buildings.[11] In comparison to the IFB model, the IFB3 model enables simultaneous structural analysis in both horizontal directions while considering elastic torsion. In the paper, the IFB3 model is first introduced (Section 2). Then, the methodology for seismic loss estimation used in this study is presented (Section 3). The methodology is based on a variant of the PEER methodology[6,7] but incorporates some modifications, which make it possible to estimate the losses directly based on the results of the response history analyses. Finally, the capability of the IFB3 model for loss estimation is verified for a contemporary frame building and an older frame building located in Ljubljana, Slovenia (Section 4). The verification involves comparing the EDPs obtained using the IFB3 and the conventional MDOF models and comparing the risk-based performance measures obtained using the two structural models.

2 | THE SIMPLIFIED MODEL FOR SEISMIC ANALYSIS OF PREDOMINANTLY PLAN-SYMMETRICAL FRAME BUILDINGS

The IFB3 model, presented in Sections 2.1 and 2.2, is an extension of the IFB model,[11] which was developed for the simulation of the 2D seismic response of contemporary and older reinforced concrete frame buildings that are predominantly plan-symmetrical. Both the IFB3 and the IFB models were defined by condensing the degrees of freedom of the conventional MDOF model. Therefore, they share many modelling assumptions, as discussed in Section 2.3.

2.1 | IFB3 model configuration

The IFB3 model is a simple 3D representation of the most important degrees of freedom of predominantly plan-symmetrical frame buildings. It consists of linear-elastic beam–column elements used to model the column and four beams per storey and nonlinear flexural plastic hinges (Figure 1A). The plastic hinges at the same storey level are referred to as an IFB3 beam–column substructure. The floors in the IFB3 model are considered rigid in their planes, and the masses and mass moments of inertia are lumped at the storey level (in the centre of mass, CM).

The IFB3 column's height is assumed to be equal to the building's storey height. The length of the IFB3 beam in a given storey and direction is defined as one half of the average length of the corresponding beams in that storey. The cross-sectional area of the IFB3 column and that of the IFB3 beams in a given storey are defined, respectively, as the sum of

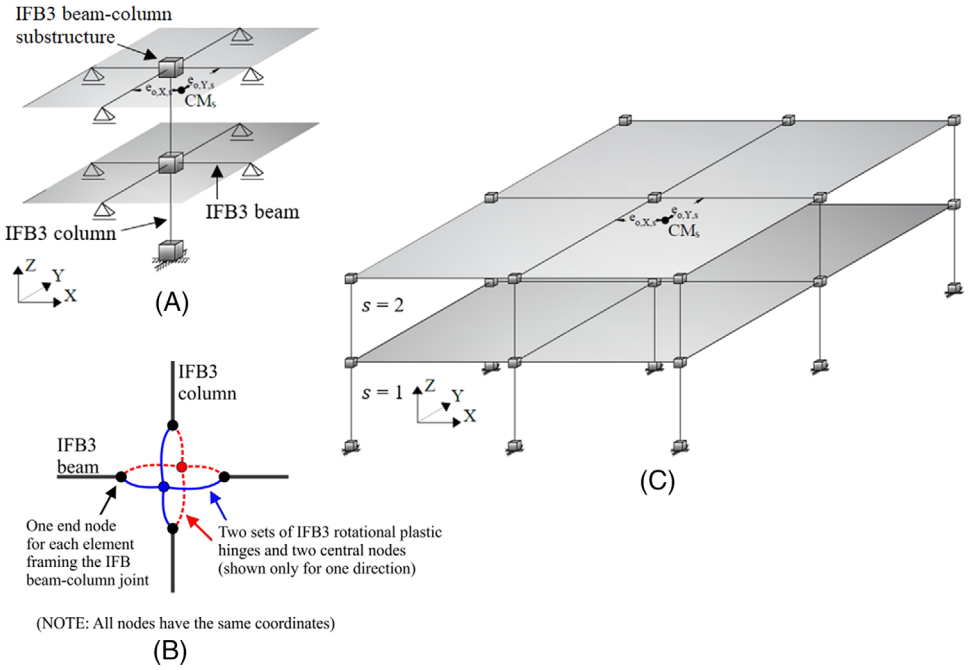

FIGURE 1 Schematic presentation of (A) the IFB3 model configuration, (B) IFB3 beam–column substructure in a middle storey for one direction only, and (C) the configuration of an MDOF model of a frame building

the cross-sectional areas of the corresponding columns and beams of the conventional MDOF model. Analogously, the moment of inertia of an IFB3 column in a given storey and direction is considered to be equal to the sum of the moments of inertia of all columns in that storey and direction. However, the moment of inertia of an IFB3 beam $I^F_{b,s}$ in a given direction and storey also approximately accounts for the effect of the variation in beam length:

$$I^F_{b,s} = \sum_{k=1}^{n} I_{b,s,k} \cdot \frac{\overline{L_{b,s}}}{L_{b,s,k}} \tag{1}$$

where the $L_{b,s,k}$ and $I_{b,s,k}$ are the length and moment of inertia, respectively, of the k-th beam in the s-th storey and the given horizontal direction of the frame building.[11] The $\overline{L_{b,s}}$ is the average length of the beams in the s-th storey that are oriented in the given horizontal direction. The effective width of the beams is determined according to Eurocode 2[29] (EN 1992-1-1:2004, 5.3.2.1), which foresees that beams are modelled as having a T cross-section with a flange width that depends on many parameters such as the beam's web thickness, the beam's length, the distance of the beam to the adjacent parallel beams and the location of the column to which the beam is connected (i.e. the internal or external column). The effective stiffness of the columns and beams is considered to be equal to 50 % of the initial stiffness of the elements according to the Eurocode 8 provisions.[30]

The modelling of the plastic hinges at the end of IFB3 beam–column elements is straightforward if the differences in the nonlinear behaviour of individual columns in a storey are not significant and if the same applies to the nonlinear behaviour of individual beams in a storey. In such cases, two plastic hinges are modelled at each end of each IFB3 column, one for the X direction and the other for the Y direction. In contrast, only one plastic hinge is modelled at the end of each IFB3 beam adjacent to the IFB3 column. The plastic hinges have zero length and connect the end nodes of the IFB3 beam–column elements with the central node in the corresponding IFB3 beam–column substructure. The central node is connected to the storey's mass node by a rigid diaphragm. According to such definition of plastic hinges, the top IFB3 beam–column substructure in Figure 1A consists of six plastic hinges (two for the column in the second storey and one for each beam in the second storey), the middle one consists of eight plastic hinges (two for the column in the first storey, two for the column in the second storey and one for each beam in the first storey), and the bottom one consists of two plastic hinges (both for the column in the first storey).

However, it was shown before[11] that using only one plastic hinge per IFB3 element and direction may not be sufficiently accurate if the damage pattern significantly varies between the building's elements framing different joints in the same

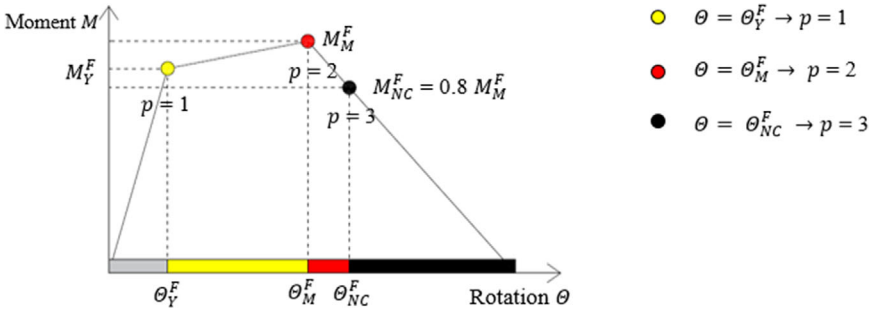

FIGURE 2 Bilinear moment–rotation relationship with linear post-capping behaviour and three characteristic points needed for its definition

storey (i.e. between the building's beam–column substructures in the same storey). Such seismic response can typically be observed in older frame buildings not designed according to the capacity design approach. The variation in the damage of the elements in the same storey causes a redistribution of seismic demands among individual beams and columns that obviously cannot be fully simulated with a simplified model where many storey's elements are condensed into a small number of elements. In the previous study,[11] this problem was addressed by reducing the strengths of individual beams before the condensation into the IFB beams so that the contribution of an individual beam to the strength of the corresponding IFB beam was limited by the strengths of the adjacent columns. This approach approximately solved the problem for frame buildings in which the ratio between the sum of the strengths of the columns and the sum of the strengths of the beams ($\sum M_c / \sum M_b$) did not vary significantly from joint to joint in a given storey. However, it was found within the present study that if $\sum M_c / \sum M_b$ varies significantly across the storey, the approach introduced before[11] may produce biased results in comparison to those observed in the conventional MDOF model. Therefore, the approach for modelling the plastic hinges in the simplified model was updated by simulating two types of beam–column substructures for each horizontal loading direction. Thus, two sets of plastic hinges are modelled in the IFB3 beam–column substructure in each storey for each direction (Figure 1B). Both sets of IFB3 plastic hinges in a given storey have the same coordinates but represent different types of the building's beam–column substructures. One set of plastic hinges represents the beam–column substructure where $\sum M_c / \sum M_b$ is less than 1, while the other one represents the substructures where $\sum M_c / \sum M_b$ is more than 1. Each set of plastic hinges is connected to a different central node, which allows to consider two different ratios between the rotations of columns and beams. The two central nodes modelled in the same storey are connected to the storey's mass node by a rigid diaphragm. Such an approach makes it possible to simulate two different damage patterns in each IFB3 beam–column substructure per direction (i.e. one with damage predominantly in the beams and one in the columns), enabling a more realistic simulation of the seismic response of within-storey irregular frame buildings than the approach introduced in,[11] where the simplified model was capable of simulating only one damage pattern per storey and direction. By adding the second set of plastic hinges into the IFB3 model, the new IFB3 beam–column substructure can be understood as a further generalisation of the IFB model.[11] However, the new IFB3 beam–column substructure is not needed to be applied at the base of the structure (where the damage is generally expected in the columns) and for buildings designed according to the capacity design approach that can be classified as within-storey regular frame buildings.

2.2 | IFB3 plastic hinges

A bi-linear moment–rotation relationship with additional linear behaviour in the post-capping range is used in IFB3 plastic hinges (Figure 2). Such plastic hinges have been proven to be sufficiently accurate for simulating the response of frame buildings up to the range of the near-collapse limit state.[10,31] The moment–rotation relationship is defined by three characteristic points ($p = 1, 2, 3$) – which refer to the yield moment (M_Y^F), the maximum moment (M_M^F) and the near-collapse moment (M_{NC}^F) – and the corresponding characteristic rotations (Θ_Y^F, Θ_M^F, Θ_{NC}^F) (Figure 2). The F in the superscript indicates that the quantity corresponds to the IFB3 model.

The characteristic moments and rotations of the plastic hinges in the IFB3 elements are defined based on the characteristic moments and rotations of the plastic hinges in the actual columns and beams of the frame, which were calculated according to a previous study.[31] The p-th characteristic moment of the h-th hinge (four hinges – top and bottom, in the X and Y direction) of the IFB3 column in the s-th storey corresponding to the t-th type of the building's beam–column substructures ($t = 1$ and $t = 2$ for substructures with ratio $\sum M_c / \sum M_b$ being less and more than 1, respectively) ($M_{c,s,h,p,t}^F$)

is calculated as the sum of the corresponding characteristic moments of individual columns ($M_{c,s,j,h,p,t}$):

$$M^F_{c,s,h,p,t} = \sum_{j=1}^{m} M_{c,s,j,h,p,t} \tag{2}$$

where index c stands for columns, j indicates the j-th column that is represented by the given IFB3 plastic hinge, and m is the number of columns represented by the given IFB3 plastic hinge. Analogously, the p-th characteristic moment of the h-th IFB3 beam (four beams oriented in the X and Y directions, as shown in Figure 1a) in the s-th storey corresponding to the t-th type of the building's beam–column substructures ($M^F_{b,s,h,p,t}$) is calculated as the sum of the corresponding characteristic moments of individual beams ($M_{b,s,k,h,p,t}$):

$$M^F_{b,s,h,p,t} = \sum_{k=1}^{n} M_{b,s,k,h,p,t} \tag{3}$$

where b in the subscript stands for beams, k indicates the k-th beam that is represented by the given IFB3 plastic hinge and n is the number of beams represented by the given IFB3 plastic hinge.

The characteristic rotations of an IFB3 column ($\Theta^F_{c,s,h,p,t}$) and IFB3 beam ($\Theta^F_{b,s,h,p,t}$) are defined as the weighted average of the characteristic rotations of the actual columns and beams represented by the IFB3 column and IFB3 beam, respectively:

$$\Theta^F_{c,s,h,p,t} = \frac{\sum_{j=1}^{m} \left(M_{c,s,j,h,p,t} \cdot \Theta_{c,s,j,h,p,t}\right)}{\sum_{j=1}^{m} M_{c,s,j,h,p,t}} \tag{4}$$

$$\Theta^F_{b,s,h,p,t} = \frac{\sum_{k=1}^{n} \left(M_{b,s,k,h,p,t} \cdot \Theta_{b,s,k,h,p,t}\right)}{\sum_{k=1}^{n} M_{b,s,k,h,p,t}} \tag{5}$$

where $\Theta_{c,s,j,h,p,t}$ and $\Theta_{b,s,k,h,p,t}$ are the characteristic rotations in individual columns and beams, respectively. Note that the weights in Equations (4) and (5) are defined by the characteristic moments of columns ($M_{c,s,j,h,p,t}$) and beams ($M_{b,s,k,h,p,t}$). The weights approximately account for the importance of the frame element in the designated storey. Different column and beam designs are thus approximately considered in the definition of the IFB3 model.

Because the IFB3 model is three-dimensional, it enables the simulation of excitations with ground motions in both horizontal directions. It also enables the consideration of elastic torsion, while the simulation of nonlinear torsion exceeds the capabilities of the model, because the latter cannot consider the progressive failure of the columns distributed along the building floor. However, even linear torsion, which occurs in predominantly plan-symmetrical buildings, can affect a building's damage and losses, where the storey drifts and storey accelerations can deviate from those in the centre of mass. The elastic torsion can be simulated if the building's mass eccentricity and torsional stiffness are accounted for. The mass eccentricity is considered by offsetting the centre of mass in each storey (Figure 1A; centre of mass CM_s is at the distances $e_{o,X,s}$ and $e_{o,Y,s}$ from the centre of rigidity). However, the torsional stiffness is prescribed to the IFB3 model by considering the torsional constant $I^F_{t,s}$ in the IFB3 column, which, for the s-th storey, is defined as:

$$I^F_{t,s} = \frac{K_{t,s} h_s}{G} \tag{6}$$

where h_s is the height of the s-th storey and G is the shear modulus and the torsional stiffness $K_{t,s}$ in the s-th storey of the IFB3 column. The torsional stiffness $K_{t,s}$ can be estimated based on the lateral stiffnesses of the frames and their distances from the centre of rigidity.[32]

The IFB3 model was added to the PBEE Toolbox,[31] which was developed in Matlab[33] for seismic response analysis of conventional MDOF models of frame buildings with OpenSees.[34] The moment-rotation relationships were modelled with Hysteretic uniaxial material. The P-delta effects were also considered.

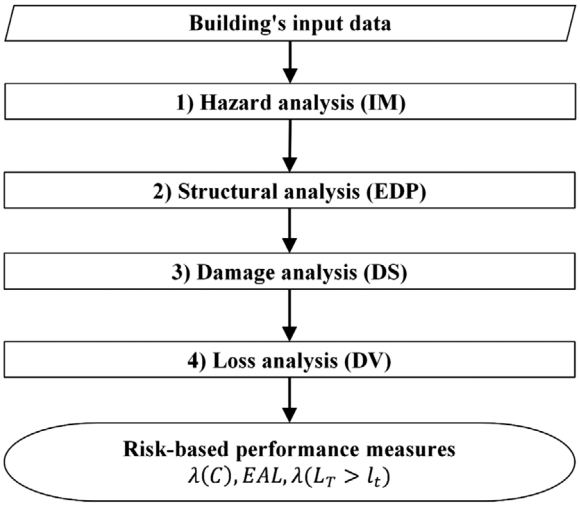

FIGURE 3 The direct loss estimation methodology algorithm (based on the PEER methodology[6])

2.3 | Comparison of the IFB3 model to the conventional MDOF model

The structural configuration of the IFB3 model is simplistic compared to that of the conventional MDOF model used in many previous studies (e.g.[9,10,31]). In the conventional MDOF model (Figure 1C), each column and beam of the frame building is explicitly modelled with a separate structural element (an elastic beam–column element with plastic hinges at its ends). In contrast, in the IFB3 model, all the elements in a given storey are condensed into a single IFB3 column and four IFB3 beams with up to two plastic hinges at their ends (Figures 1A and 1B and Section 2.1). Due to this simplification, the IFB3 model has more limitations than the conventional MDOF model. It does not enable the simulation of nonlinear torsion. Also, it is unable to correctly simulate the seismic response of frames with highly irregular beam lengths. Therefore, it is principally intended for predominantly plan-symmetrical frame buildings, where the variation in beam length is not extremely high. Moreover, the IFB3 model does not account for the effects of varying axial forces (due to overturning) on the column moment capacity, which can become especially important in the case of one-bay frames or frames with a height–length ratio greater than three.[18]

However, there are also many similarities between the IFB3 and the conventional MDOF model. The level of input data required to define both models can be the same. The models also share several modelling assumptions. In both cases, the masses are assumed to be lumped at the storey level, floors are assumed to be rigid in their plane, and the structural elements are modelled as beam–elastic elements with plastic hinges at their ends. Moreover, both models simulate the nonlinear response of the building structure based on the concentrated plasticity approach. The same formulation of the plastic hinges can be used in both models.

Furthermore, both models require that an assumption is made regarding the effective beam widths and the effective stiffness of columns and beams in cases where the cracking of concrete is not considered in the plastic hinges. The nonlinear shear, torsional and axial behaviour of individual structural elements, which is neglected in the IFB3 model, is also usually not considered in the conventional MDOF model. Another limitation of the IFB3 model is that the nonlinear response of the beam–column joints is not simulated. This limitation is also embedded in the conventional MDOF model, as defined in this paper. However, it should be noted that several similar MDOF models explicitly account for the beam–column joints.[35–37]

3 | DIRECT SEISMIC LOSS ESTIMATION METHODOLOGY

The direct seismic loss estimation is based on a variant of the PEER methodology[6] that consists of four different types of analysis (Figure 3), namely hazard analysis, structural analysis, damage analysis and loss analysis, and follows the algorithm proposed by Snoj and Dolšek.[7] This algorithm is based on the direct estimation of damage and loss from the structural analysis results, thus explicitly considering the correlation between damage occurring in different components. However, in contrast with,[7] where the EDPs were obtained by a response history analysis of the SDOF model and a

pushover analysis of the MDOF model, the EDPs in this study were obtained directly from the response history analysis of the IFB3, and, for the purpose of comparison, by the response history analysis of the conventional MDOF model as well.

In the following subsections, the description of the direct loss estimation methodology focuses on the structural, damage and loss analyses, which depend on the definition of the structural model (i.e. IFB3 or the conventional MDOF model). However, for completeness, the hazard analysis is also briefly presented. The steps of the loss estimation are presented in Sections 3.1–3.4, followed by the description of the performance measures used in this study (Section 3.5).

3.1 | Hazard analysis

The seismic hazard analysis enables the estimation of the frequency of the exceedance of different levels of seismic intensity at the building's site, $\lambda(IM > im)$, which is represented by the seismic hazard curve. The analysis is based on the seismological properties at the building's location, the local soil properties, nearby earthquake sources, and ground-motion models, which determine the IM value based on the magnitude, distance and other relevant parameters. In addition to the seismic hazard curve, the hazard analysis also provides the basis for the selection of ground-motion records for the subsequent structural analysis (see also application in Section 4).

3.2 | Structural analysis

In this study, the structural analysis was performed using a nonlinear response history analysis of the IFB3 model and the conventional MDOF model. A set of hazard-consistent ground motions was utilised. The ground motions were scaled to various levels of intensity measure (IM) until the collapse intensity was reached.[38] The ground-motion randomness was thus explicitly considered in the analysis. However, for simplicity, the modelling uncertainties related to the structural model were disregarded.

In each simulation, defined by the index of the ground motion (a) and the index of the IM level (i), an array of the maximum EDPs $\{edp_{a,i,1}, \dots, edp_{a,i,j}, \dots, edp_{a,i,n_{comp}}\}$ is obtained, where $edp_{a,i,j}$ is the value of the EDP relevant for the simulation of damage in the j-th building component (e.g. inter-storey drift, storey acceleration, plastic hinge rotation) obtained for the a-th ground motion at the i-th level of IM, and n_{comp} is the number of all building components. Another result of the simulations is the value of collapse intensity, determined for each ground motion considered. The collapse intensity for the a-th ground motion is denoted as $im_{C,a} = IM(i_{C,a})$, where $i_{C,a}$ is the index of the collapse level of IM for the a-th ground motion. Based on the collapse intensities for all ground motions, the collapse fragility function can be estimated, which describes the probability of collapse given the value of $IM = im$, $P(C|IM = im)$. The estimation of the collapse fragility function based on a set of collapse intensities can be performed using different techniques, as described, for example, by Baker.[39] Note that the collapse fragility function is not needed in the loss estimation as performed in this study. However, it was nonetheless estimated in the example presented in Section 4 to further estimate the frequency of collapse, which is often used to describe the seismic performance of buildings.

The response history analyses provide EDPs at a limited number of IM levels. The EDPs at other IM levels are thus estimated by linear interpolation based on EDPs from the response history analysis $\{edp_{a,1}(im), \dots, edp_{a,j}(im), \dots, edp_{a,n_{comp}}(im)\}$, where $edp_{a,j}(im)$ is the value of the EDP relevant for the simulation of damage in the j-th building component obtained for the a-th ground motion at $IM = im$. The definition of EDPs for any IM values (not just at the levels considered in the response history analyses) is important for two reasons. Firstly, it allows for a finer discretisation of the IM domain, and secondly, it enables EDPs to be estimated at the same levels of IM for each ground motion.

3.3 | Damage analysis

The damage analysis is aimed at estimating the damage to building components. Only simulations from the non-collapse cases ($IM < im_{C,a}$) are considered in the damage analysis. Detailed damage analysis of individual building components is not required in the collapse cases because the building needs to be replaced. The damage analysis is performed for each array $\{edp_{a,1}(im), \dots, edp_{a,j}(im), \dots, edp_{a,n_{comp}}(im)\}$ determined in the structural analysis. The results of the damage analysis are the occurrence probabilities of building components' damage states. For a given

ground motion (a) and $IM = im$, these occurrence probabilities can be represented by an array of probability vectors $\{p_{DS,a,1}(im), \dots, p_{DS,a,j}(im), \dots, p_{DS,a,n_{comp}}(im)\}$, where $p_{DS,a,j}(im)$ is the vector of occurrence probabilities of the damage states designated for the j-th building component. For the d-th damage state of the j-th building component, the occurrence probability is defined as[2]:

$$p_{DS,d,a,j}(im) = P(DS_j = ds_d | EDP_j = edp_{a,j}(im)) = \begin{cases} 1 - P(DS_j \geq ds_{d+1} | EDP_j = edp_{a,j}(im)), & \text{if } d = 0 \\ P(DS_j \geq ds_d | EDP_j = edp_{a,j}(im)) - P(DS_j \geq ds_{d+1} | EDP_j = edp_{a,j}(im)), & \text{if } 1 \leq d < m_j \\ p(DS_j \geq ds_d | EDP_j = edp_{a,j}(im)), & \text{if } d = m_j \end{cases} \quad (7)$$

where DS_j is a discrete random variable that describes the damage state of the j-th building component, EDP_j is the corresponding EDP, $P(DS_j \geq ds_d | \ EDP_j = edp_{a,j}(im))$ is the fragility function for damage state ds_d evaluated for $EDP_j = edp_{a,j}(im)$ and m_j is the index of the most severe damage states of the j-th building component. The total number of damage states for the j-th building component, including the no-damage state ($d = 0$), is thus $m_j + 1$.

3.4 | Loss analysis

The objective of the loss analysis is to estimate the expected total loss of the building given the ground motion and the level of IM. The collapse and non-collapse cases are usually treated separately. In this study, the expected total loss for the collapse (C) cases, $E(L_{C,a}(im))$, was considered to be equal to the expected replacement cost, $E(L_C)$, which accounts for additional demolition work and site clearance.[1,4,7] The value of $E(L_C)$ was considered to be 110 % of L_{new}, where L_{new} is the cost of a new building.[7] $E(L_C)$ was assumed to be independent of the ground motion and the IM value.

For the non-collapse (NC) cases, the losses resulting from the damage to individual building components first need to be estimated. This is done by coupling the occurrence probabilities of damage states obtained in the damage analysis with the loss functions. The loss functions herein are defined by the expected normalised loss given the damage state, $E(L_j^{'} | \ DS_j = ds_d)$, where the normalised loss ($L_j^{'}$) represents the ratio of the repair cost of the j-th component ($c_{repair,j}$) to the cost of a new component ($c_{new,j}$).[7] For the j-th building component, a-th ground motion and $IM = im$, the expected normalised loss $E(L_{a,j}^{'}(im))$ is calculated as:

$$E\left(L_{a,j}^{'}(im)\right) = \sum_d E\left(L_j^{'} | DS_j = ds_d\right) \cdot P\left(DS_j = ds_d \mid EDP_j = edp_{a,j}(im)\right) \quad (8)$$

It should be noted that in a more detailed loss analysis, also aimed at estimating the dispersion of losses for a given ground motion and IM value, the loss functions would also have to consider the uncertainty in $L_j^{'} | \ DS_j = ds_d$ (not just its expected value). Furthermore, the correlation between the damage states of different components and the correlation between losses of different components would need to be prescribed. For simplicity, this information was disregarded in the present study.

Based on $E(L_{a,j}^{'}(im))$, the quantity of the j-th component (q_j) and the cost of a new j-th component per unit ($c_{new,j}$), the expected loss of the j-th component for a given ground motion a and IM level, $E(L_{a,j}(im))$, can be evaluated[7] as:

$$E\left(L_{a,j}(im)\right) = q_j \cdot E\left(L_{a,j}^{'}(im)\right) \cdot c_{new,j} \quad (9)$$

By applying Equation (9) to each building component, an array of losses $\{E(L_{a,1}(im), \dots, E(L_{a,j}(im), \dots, E(L_{a,n_{comp}}(im)\}$ is obtained. The expected loss at the building level for a given ground motion, IM level and the NC case, $E(L_{NC,a}(im))$, can then be calculated simply by summing the elements of that array:

$$E\left(L_{NC,a}(im)\right) = \sum_j E\left(L_{a,j}(im)\right) \quad (10)$$

However, the total expected loss as defined by Equation (10) can be directly applied only in non-collapse cases in which a building is restored by repairing or replacing the damaged components. To account for other restoration strategies, two types of adjustments were considered in this study. The first type of adjustment was applied if $E(L_{NC,a}(im))$ was higher than the threshold for economically justified renovation (L_{tr}). In such cases, it was assumed that the building would be

replaced. The total expected loss was thus considered to be equal to the building's replacement cost, $E(L_C)$. The value of L_{tr} was assumed based on existing guidelines and documents. Namely, FEMA P-58-1[6] suggests that the owners will most likely elect to replace a building when the projected repair costs exceed 40 % of the replacement cost. A threshold of 40 % was also adopted in the Slovenian program for reconstruction after the 2004 earthquake in the Upper Posočje, but in this case, the threshold corresponded to the cost of a new building.[40] Therefore, in this study, L_{tr} was also considered to be 40 % of the cost of a new building.

The second adjustment was applied when the seismic intensity was very low. In such cases, as the post-earthquake analysis[41] shows, buildings are at most only slightly damaged, which means it is unlikely that the stakeholders will decide to repair them. Therefore, a lower boundary for the seismic intensity (im_{min}) was applied under which the total expected loss was considered to be equal to 0. The boundary was defined in terms of the elastic spectral acceleration ($S_{ae,min}$) according to FEMA P-58-1.[6] If the average of the fundamental periods in both horizontal directions ($\bar{T}$) was less than 1.0 s, $S_{ae,min}$ was set to 0.05 g. Otherwise, $S_{ae,min}$ was set to 0.05 g/$\bar{T}$.

By considering that the occurrence of non-collapse and collapse cases depends on whether the IM is lower or higher than $im_{C,a}$, and by adopting the two types of adjustments for the non-collapse cases, the total expected loss for any given ground motion and IM value can be written using the following general equation:

$$E\left(L_a\left(im\right)\right)=\begin{cases}0, & \text{if } IM<im_{\min}\\ E\left(L_{NC,a}\left(im\right)\right), & \text{if } IM<im_{C,a} \text{ and } E\left(L_{NC,a}\left(im\right)\right)<L_{tr}\\ E\left(L_C\right), & \text{if } IM<im_{C,a} \text{ and } E\left(L_{NC,a}\left(im\right)\right)\geq L_{tr}\\ E\left(L_C\right), & \text{if } IM\geq im_{C,a}\end{cases} \tag{11}$$

3.5 | Estimation of risk-based performance measures

In this study, three risk-based performance measures were considered. The first one is the mean annual frequency of collapse $\lambda(C)$. This performance measure is not actually related to losses, but it was evaluated nonetheless because it is often used to communicate the seismic performance of buildings (e.g.[2,7]). The $\lambda(C)$ is defined as:

$$\lambda\left(C\right)=\int_0^\infty P\left(C|IM=im\right)\left|\frac{d\lambda\left(IM>im\right)}{dIM}\right|dIM \tag{12}$$

In Equation (12), $P(C|IM=im)$ is the building's collapse fragility function and $|\frac{d\lambda(IM>im)}{dIM}|$ presents the absolute value of the derivative of the seismic hazard curve. The second risk-based performance measure is the expected annual loss (EAL), which can be calculated as:

$$EAL=\int_0^\infty E\left(L\left(im\right)\right)\left|\frac{d\lambda\left(IM>im\right)}{dIM}\right|dIM \tag{13}$$

where $E(L(im))$ is the mean of $E(L_a(im))$ over all considered ground motions. Finally, the third performance measure considered in this study is the mean annual frequency of exceedance of a specified loss value, $\lambda(L>l)$, that is the loss curve, which can be estimated as:

$$\lambda\left(L>l\right)=\int_0^\infty P\left(L>l|IM=im\right)\left|\frac{d\lambda\left(IM>im\right)}{dIM}\right|dIM \tag{14}$$

where $P(L>l|IM=im)$ is the probability that the total loss exceeds the designated loss value (l) at a given intensity (im). This probability is defined herein as the complementary cumulative distribution function of total expected losses determined for individual ground motions, $E(L_a(im))$. Therefore, it accounts for the record-to-record randomness and uncertainties in the damage simulation captured within the components' fragility functions but neglects the modelling uncertainties related to the structural response and the uncertainties in loss functions.

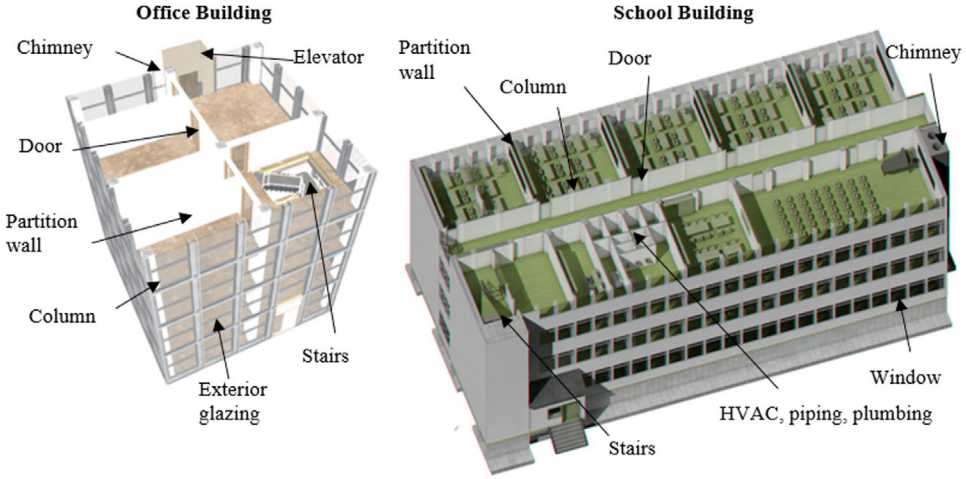

FIGURE 4 Presentation of the building information models of the analysed office and school buildings

4 | APPLICATION OF THE IFB3 MODEL IN DIRECT SEISMIC LOSS ESTIMATION

In this section, the estimated seismic losses are presented for two frame buildings, which were analysed using the IFB3 model and the conventional MDOF model. The goal of this application was to demonstrate loss estimation using the IFB3 model and to investigate the capability of the IFB3 model in seismic loss estimation compared to that based on the conventional MDOF model.

4.1 | Analysed buildings, seismic hazard and ground motions

Loss estimations were performed for a four-storey office building and a five-storey school building, both located in Ljubljana, Slovenia. The structure of the office building was considered equal to the four-storey plan-symmetrical reinforced concrete frame building presented in a previous study.[42,43] The rooms are separated by the gypsum partition walls, while the outer perimeter of the building represent exterior glazing (Figure 4). Suspended acoustic ceiling panels are installed on all storeys. An elevator is located on the outside of the building. Moreover, the school building includes classrooms, offices, bathrooms and a library on the first four storeys (Figure 4) and a gym in the attic (the fifth storey). The rooms are separated by partition walls with no openings, or with openings for the doors. Most of the façade is covered by windows. For easier representation, building information models of the analysed buildings were developed with ArchiCAD software v.22[44] (Figure 4).

For the office building (Figure 5A), a building structure that had been pseudo-dynamically tested at the ELSA Laboratory[42,43] was considered. It was designed according to the pre-standard of the current Eurocode 8 with consideration of ductility class high, design PGA = 0.3 g and medium soil conditions. The total horizontal design force was estimated equal to 15 % of the building weight.[42] For the design and construction of the building, concrete C25/30 and Tempcore reinforcing bars class B500 were used.[42,43] The characteristic and design compressive strength of concrete and reinforcing bars amounted, respectively, to 25 and 14.2 MPa, and 500 and 435 MPa. The building was designed according to the ultimate limit state design approach as prescribed in the pre-standard of Eurocode 2. This approach foresees that members are designed so that the design strength of each cross-section is greater than the design action effect in that cross-section (usually in terms of internal forces). The mass of the building was 342 t. The mean concrete strength and the mean yield strength of the reinforcement used later in the analysis were equal to 42 and 580 MPa, respectively.[31] The cross-sectional dimensions of the columns were 40/40 cm and 45/45 cm, and their total reinforcement ratio in the bottom storey was about 1.6 %.

The school building (Figure 5B) was designed in 1963 and built in 1965 in Ljubljana, Slovenia. The building was designed following the Yugoslavian temporary regulation for concrete and reinforced concrete buildings[45] and the first Slovenian seismic code, implemented in 1963.[46] The regulations at the time of the building design followed the so-called allowable stress design approach, where the structural elements were designed according to the prescribed allowable stresses of

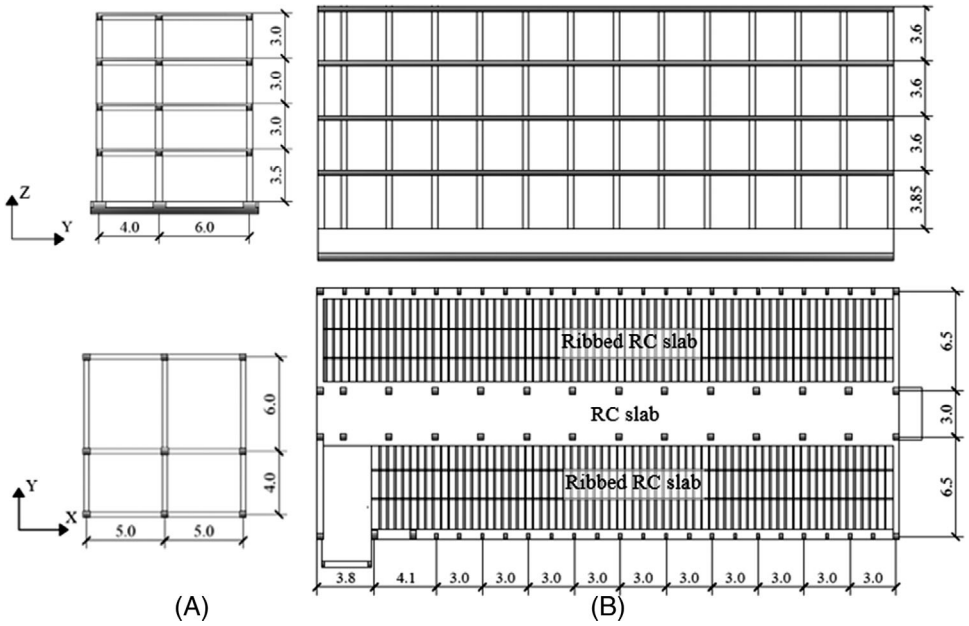

FIGURE 5 The elevation and plan views of (A) the office building and (B) the school building

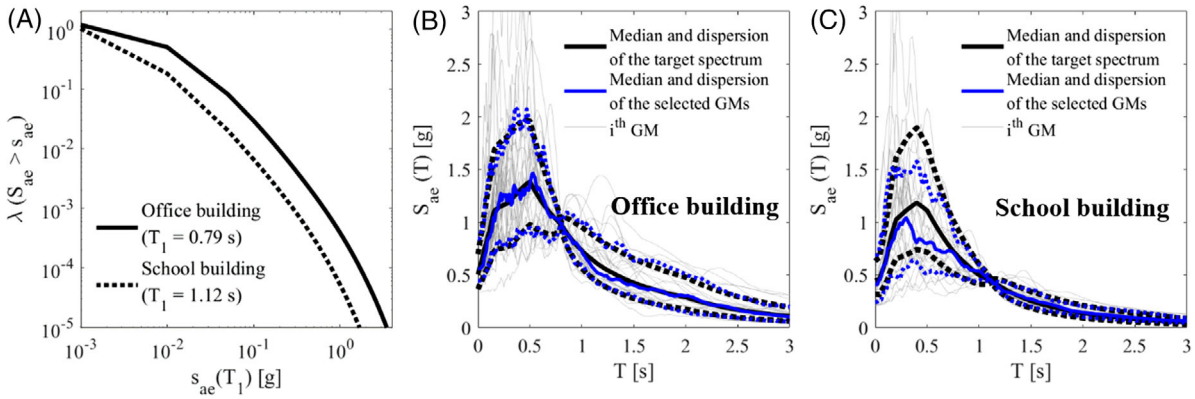

FIGURE 6 (A) The seismic hazard curves for the locations of the investigated buildings and the target conditional spectrum and the acceleration spectra of the selected ground motions (GMs) for (B) the office building and (C) the school building

concrete and reinforcement. The allowable stresses depended on the type of action effect (i.e. tension, pressure, bending or shear), type of structural element (i.e. slab, beam or column) and characteristic strength of the material.[45] The mean concrete strength varied between 25 and 32 MPa, while the elastic modulus of the concrete was between 29 and 31.8 GPa. The mean yield strength of reinforcement (276 MPa) was estimated by increasing the characteristic strength by 15 %, according to Eurocode 8-2.[47] In the design of the building, the base shear force was estimated to be equal to 11 % of the building weight.[46] The mass of the building, as determined using the building information model, was equal to 2710 t. In the structural analysis, only the bottom four storeys were considered (RC frames), because the fifth storey contains only a wooden frame structure. The cross-sectional dimensions of the columns are 20/40 cm in the outside frames and 40/40 cm in the inner frames (Figure 5B). The corresponding total reinforcement ratios in the bottom storey amount to 1.0% and 0.95%, respectively, much less than in the case of the office building.

The seismic hazard curves were determined based on the official probabilistic seismic hazard maps for Ljubljana, Slovenia.[48] They correspond to spectral accelerations at the fundamental periods of the office building (0.79 s) and the school building (1.12 s) and to soil types B and C, respectively.[30] Based on the seismic hazard, 30 ground motions (Figure 6), which were later used in the structural analysis, were selected. The selection of ground motions was based on a target spectrum and an algorithm proposed in.[49] For the target spectrum, the conditional spectrum (CS)[50] was used. It was defined based on the mean magnitude and distance resulting from the disaggregation of seismic hazard for the mean return

period of 2475 years. The ground motions were obtained from the NGA[51] and RESORCE[52] databases. In the ground-motion selection, the geometric mean of the spectral accelerations of the two horizontal ground-motion components was considered.

4.2 | Structural analysis

The EDPs were evaluated based on the response history analyses utilizing the IFB3 model and the conventional MDOF model. It should be noted that the IFB3 model of the school building and that of the office building had different numbers of plastic hinges per storey and direction. The school building was classified as a within-storey irregular frame building because both types of beam–column substructures were observed in that building (i.e. the ratio $\sum M_c/\sum M_b$ below and above 1). Consequently, two sets of plastic hinges (Figure 1B) were modelled in each IFB3 beam–column substructure above the ground level. However, at the ground level, where the damage can occur only in the columns, as discussed in Section 2.1, only one set of IFB3 plastic hinges was modelled. In contrast, one set of plastic hinges was modelled in all IFB3 beam–column substructures of the office building because this building was classified as a within-storey regular building (i.e. the ratio $\sum M_c/\sum M_b$ was generally above 1), as is usually the case with frame structures designed according to the capacity design approach.

For the office building, some ground motions had to be scaled to extremely high IM levels to observe collapse. Thus, the truncated IDA[38] was utilised. The maximum IM level was estimated at an intensity of $S_{ae} = 2.5$ g, considering that potential earthquakes with intensity levels higher than $S_{ae} > 2.5$ g do not contribute significantly to the estimation of risk-based performance measures in Slovenia. For the office building and for $S_{ae}(T_1)$ equal to 2.5 g, the 16^{th}, 50^{th} and 84^{th} percentile ground-motion scale factors were equal to 5.9, 8.9 and 15.2, respectively. For the school building, the scale factors were lower. At the collapse of the building, their 16^{th}, 50^{th} and 84^{th} percentile values amounted to 0.7, 1.1 and 2.2, respectively, if using the IFB3 model. The scale factors obtained with the MDOF model were only slightly different due to similar collapse intensities, as presented later in this section. Although the ground-motion scale factors in the case of the office building can provide some bias in the prediction of the EDPs (e.g.[53]), this issue was not further investigated in the present study because the main objective was to demonstrate the capability of the simplified structural model relative to that of the conventional MDOF model.

The procedure for the evaluation of the EDPs depended on the type of structural model and the building component type (structural or non-structural). In the case of the conventional MDOF model, the EDPs related to the structural components (e.g. rotations in plastic hinges) were recorded directly from the response history analyses. However, the EDPs at the locations of non-structural components were estimated by linearly interpolating the response histories of the EDPs (i.e. inter-storey drifts and floor accelerations) of the closest structural components. In the case of the IFB3 model, the rotations in plastic hinges of structural components were not available due to the reduced degrees of freedom of the IFB3 model. Therefore, the damage to structural components was estimated based on the rotation demand in the plastic hinges of the IFB3 elements, as explained in Section 4.3. However, the calculation of inter-storey drifts and floor accelerations at the locations of non-structural components was based on kinematic quantities (i.e. response histories of inter-storey drifts and floor accelerations) at the centreline of the IFB3 column at each storey level and by assuming a rigid diaphragm at each floor of the building.

The obtained EDPs were then used to define the IDA curves. The spectral acceleration at the building's fundamental period $S_{ae}(T_1)$ was adopted for the IM for consistency with the IM considered in the hazard analysis. However, the IDA curves were constructed for different EDPs, such as the maximum inter-storey drift and the maximum storey acceleration at the centre of mass (CM), which are presented in Figure 7 to the point of the building's collapse as defined later in this section. In addition to the single IDA curves, the percentile IDA curves are also presented in Figure 7. However, they do not affect further loss estimation, as the latter is based on single IDA curves.

Regardless of the significant simplification considered in the IFB3 model, it can be observed that the IDA curves based on the IFB3 model and the conventional MDOF model were similar. It can also be observed that a considerable amount of IDA curves representing the relationship between the spectral acceleration and maximum inter-storey drift are similar to a linear function. This observation is the consequence of relatively long fundamental periods of the investigated buildings for which it is well known that the 'equal displacement rule' applies.[54–56] In contrast, the slope of the IDA curves for the maximum storey acceleration increases as the structure goes from the linear to the nonlinear range, indicating a slower increase of storey accelerations with the seismic intensity. For more confidence in the results, the maximum storey

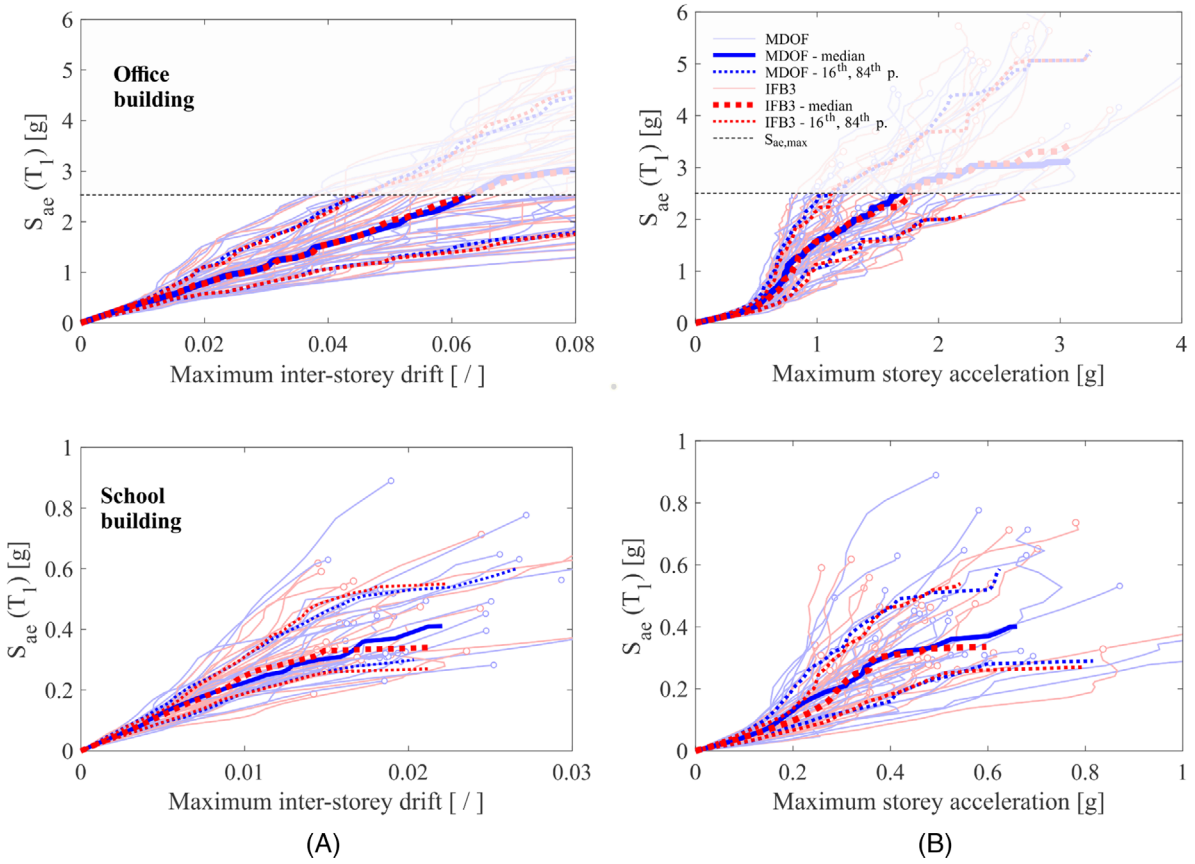

FIGURE 7 The IDA curves of each considered ground motion and the median, 16th and 84th percentile IDA curves for the IFB3 model and the conventional MDOF model of the office building and the school building: (A) for the maximum inter-storey drift, (B) for the maximum storey acceleration

accelerations in the elastic range were also verified with a simplified method for estimating floor acceleration spectra,[57] which gave very similar results.

Another result of the structural analysis relates to the sample of collapse intensities. Several definitions of the collapse of a building are available in the literature.[8,58] In this study, the collapse of the building within IDA was defined by the maximum inter-storey drift of the MDOF or IFB3 model exceeding 10 %,[58] which also accounted for cases of global dynamic instability (i.e. cases in which the maximum inter-storey drift increased over all limits during the nonlinear response history analysis). However, because both structural models can be considered simplified, another collapse criterion was defined based on the severe strength degradation of individual columns. It was assumed that a column reaches the collapse limit state when its bending strength drops to 50 % of the maximum moment (M_M) on the linear softening branch of the moment–rotation relationship. The building collapse was assumed to take place when the first column reached a collapse limit state defined in this way. For the conventional MDOF model, verifying the second collapse criterion was straightforward because seismic demand and capacity were calculated explicitly for each column. On the contrary, the IFB3 model is not capable of simulating the seismic demands and capacities of individual columns directly. However, the issue was approximately solved by post-processing IDA results. In the post-processing, the collapse of the IFB3 model was considered attained if the seismic demand in an IFB3 column exceeded the minimum of the collapse capacities of all columns condensed into that IFB3 column.

The collapse fragility functions were defined by the sample-based cumulative distribution function considering collapse intensities ($im_{C,a}$). Additionally, the lognormal cumulative distribution function was also estimated, as in many other studies.[9,11,38,59,60] For both the IFB3 model and the conventional MDOF model, the collapse fragility functions are presented in Figure 8. It can be observed that the collapse fragility functions estimated with different structural models were very similar for the office building. However, for the school building, the differences in the collapse intensities varied. In the range of collapse probabilities around 0.50, the differences amounted to about 15–18%, while for other collapse

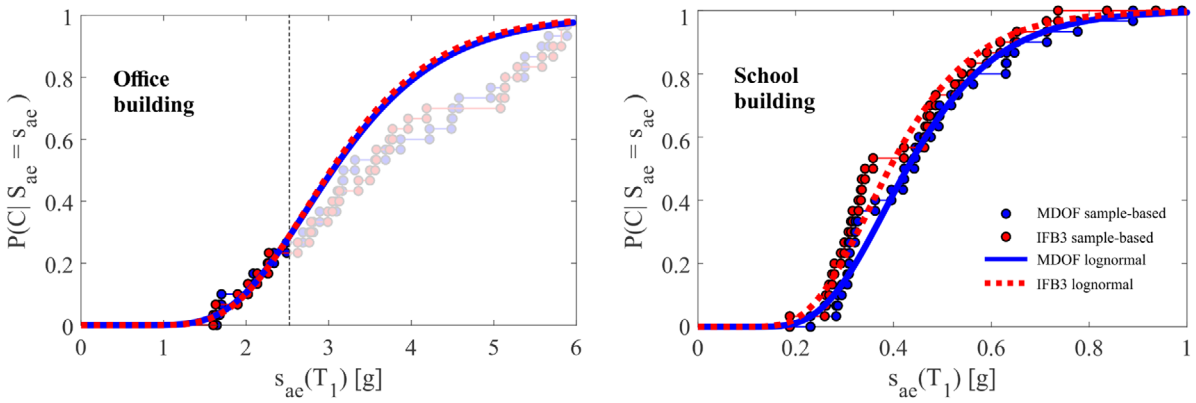

FIGURE 8 The sample-based collapse fragility functions and the fragility functions utilizing the lognormal cumulative distribution function for the office building and the school building analysed by the IFB3 model and the conventional MDOF model

probabilities, the differences were lower and comparable to those observed for the office building. Consequently, the lognormal fragility functions obtained with the two structural models were similar also in this case.

The computational time differed significantly despite the similarity between the structural analysis results obtained with the two structural models. In the case of the office building, the IDA using the IFB3 model was performed in 13.0 hours on a computer with Intel(R) Xeon(R) CPU L5520 @ 2.26 GHz and 8 GB of system RAM, which is only 4.3-times faster than the computational time needed in the IDA utilising the conventional MDOF model (56.1 hours). However, in the case of the relatively complex school building, the computational time differed by a factor of about 580. With the IFB3 model, the total computational time on one computer amounted to 14.1 hours, while with the conventional MDOF model, the computation time increased to 8175 hours. Thus, it was necessary to use a grid of computers to make IDA based on the MDOF model feasible.

4.3 | Damage analysis

A set of EDP-based fragility functions characterised the probabilities of the exceedance of damage states for the building components conditional to the EDPs. They were formulated as lognormal cumulative distribution functions as an input for damage analysis and represent the capacity of building components for discrete damage states. Each fragility function is defined by the median $\widetilde{EDP}_{d,j}$ and the logarithmic standard deviation $\beta_{DS,d,j}$, where d and j refer to the damage state and the component, respectively. Two different approaches were utilised for defining these parameters of the fragility functions. For the non-structural components, the parameters were obtained from the literature.[1–7,61,62] They are presented in the Appendix. However, for the structural components (i.e. reinforced concrete columns and beams), the medians, $\widetilde{EDP}_{d,j}$, were defined based on the characteristic rotations in plastic hinges Θ_p (Figure 2). For each column and beam, five damage states were defined ($ds_0 - ds_4$), including the no-damage state (ds_0). Damage state ds_1 corresponded to the first characteristic rotation in the plastic hinge of the structural component ($\Theta_{p=1}$), damage state ds_2 to $(\Theta_{p=1} + \Theta_{p=2})/2$, damage state ds_3 to $\Theta_{p=2}$ and damage state ds_4 to $\Theta_{p=3}$ (see Figure 2). In this way, it was considered that the fragility of each structural component depended on the cross-sectional properties that affected the plastic hinges. However, the corresponding logarithmic standard deviations $\beta_{DS,d,j}$ were, as in the case of the non-structural components, obtained from the literature. For ds_1, the logarithmic standard deviation corresponding to the damage state characterised by the degradation of the initial elastic stiffness of the columns and beams (0.36 [63,64]) was considered. For ds_4, the logarithmic standard deviation corresponding to a 20 % drop in the element's strength in the post-capping range (0.40 for the columns,[63] 0.60 for the beams[64]) was taken into account. However, for ds_2 and ds_3, no directly applicable values were found in the literature. Therefore, the same values as those considered for ds_1 and ds_4, respectively, were applied.

The definition of EDP-based fragility functions for columns and beams depended on the type of structural configuration considered in the models (Figure 1). Specifically, the number of plastic hinges in the IFB3 model was lower than in the conventional MDOF model, which included all columns and beams. Therefore, the number of fragility functions was also different. To better understand the difference, the probabilities of damage states for column hinges that were observed most vulnerable are presented in Figure 9A. In the case of the office building, the most vulnerable hinges were located at

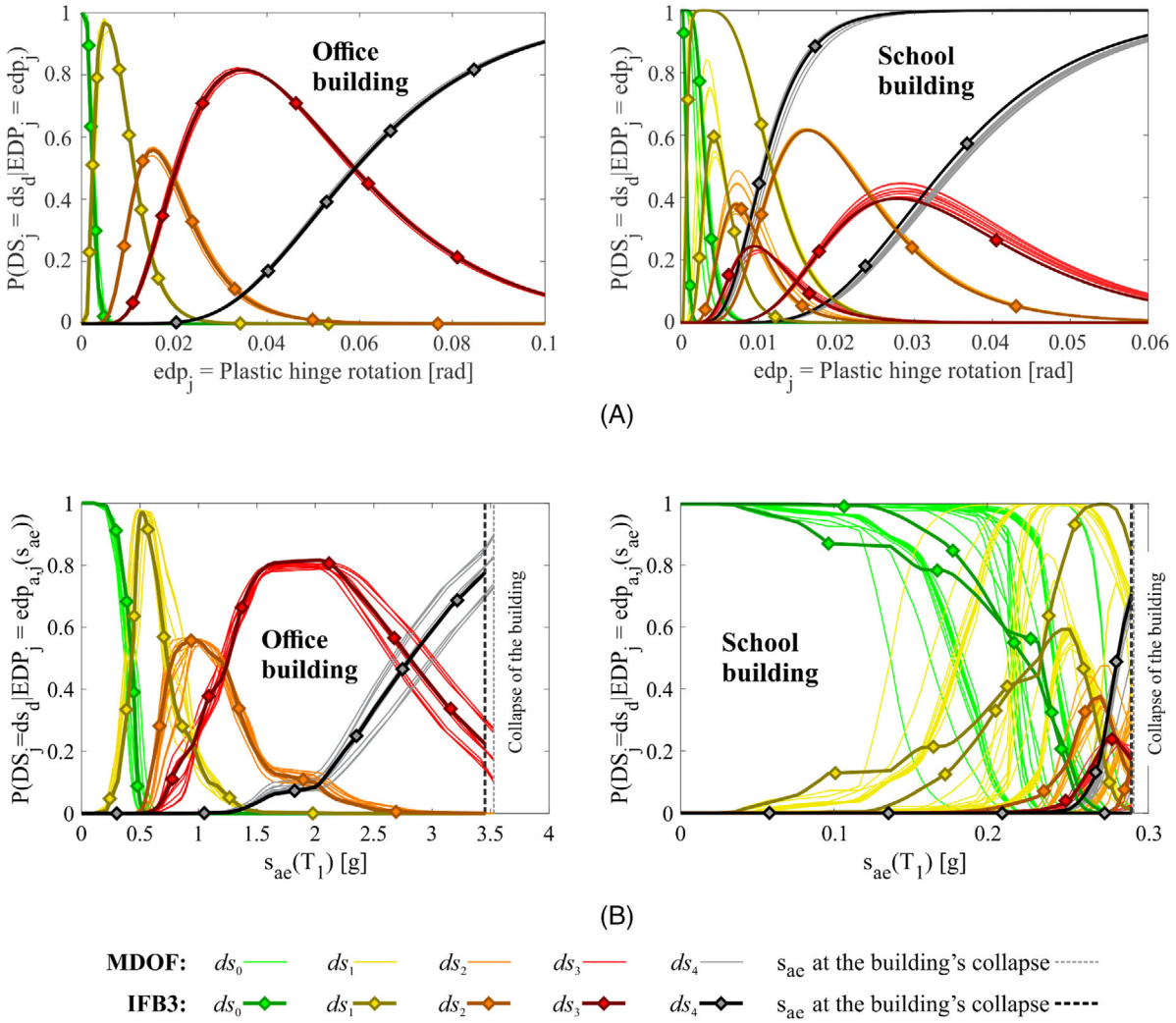

FIGURE 9 Damage state probabilities of the columns at the base of the office building and at the bottom of the top-storey of the school building estimated with the IFB3 model and the conventional MDOF model. (A) The probabilities are conditional to the EDP and represent the input for the damage analysis, (B) the probabilities are conditional to the IM and the selected characteristic ground motion and represent the outcome of the damage analysis

the base of the building, while for the school building, they were located at the bottom of the top storey (in both cases in the X direction). The damage-state probabilities presented in Figure 9A were determined directly from the EDP-based fragility functions (Equation (7)). In the case of the conventional MDOF model, the number of curves per damage state is equal to the number of columns in a storey (i.e. nine for the office building and 80 for the school building). This is because all columns are explicitly modelled in the conventional MDOF model. For the office building, it can be observed (Figure 9A) that the damage state probability curves for a given damage state approximately overlap due to the small variation in the design and geometry of columns at the base. In contrast, two groups of damage state probability curves for a given damage state can be observed for the school building (Figure 9A) because of the significantly different geometry of the perimeter and internal columns (Figure 5). However, in the case of the IFB3 model, only one and two damage state probability curves for a given damage state are considered, respectively, for the office and school building. The consideration of two damage state probability curves per damage state in the case of the school building is a consequence of using two sets of plastic hinges in the IFB3 beam–column substructure. For both buildings, good matching between the IFB3 probability curves and the MDOF probability curves can be observed (Figure 9A), which is a direct consequence of the definition of the characteristic rotations in the IFB3 model (Equation (4)).

The EDPs from the response history analyses (i.e. the demand) and the damage state probabilities presented in Figure 9A (i.e. the capacity) were used to calculate the damage state probabilities conditional to the IM ($p_{DS,d,a,j}(im)$

(Equation (7)). The IM-based damage state probabilities represent the outcome of the damage analysis and, as an example, are presented in Figure 9B for the most vulnerable column hinges by analogy to Figure 9A. Because the IM-based damage state probabilities were determined for each ground motion separately, the total number of the corresponding curves was 30-times higher than in the case of the EDP-based damage state probabilities shown in Figure 9A. Therefore, for the sake of clarity, the IM-based damage state probabilities are in this section presented for only one ground motion, hereinafter denoted as the characteristic ground motion (Figure 9B). However, note that the damage and loss analyses were performed for 30 selected ground motions per building. In general, it can be observed that the variability of the IM-based damage state probabilities (Figure 9B) was more pronounced than the variability of the EDP-based damage state probabilities (Figure 9A). This is because the variation in the geometry and design of columns also affects the seismic demand (i.e. the EDPs), which impacts the IM-based damage state probabilities. The variability of the IM-based damage state probabilities was higher in the case of the school building due to the more pronounced torsional response and larger differences between the columns.

Moreover, the IM-based damage state probabilities for the office building obtained with the conventional MDOF model were scattered around those obtained with the IFB3 model, indicating good matching between the results produced by the two structural models. In the case of the school building, the scatter of IM-based damage state probabilities for the office building was significantly higher than that of the office building. The matching between the curves obtained with the two models was still quite similar for more severe damage states but not so similar for slighter damage states (e.g. for ds_1), indicating that IFB3 model produced some bias in the estimation of rotations of plastic hinges. However, this bias was not very high and did not significantly impact the risk-based performance measures, as shown in Section 4.5. It is also interesting to note that, in the case of the school building, the IM-based damage state probabilities rise notably above 0 for both considered IFB3 plastic hinges only for damage states ds_1, ds_2 and ds_3, but not for damage states ds_4 and ds_5. This observation is consistent with the results obtained with the conventional MDOF model, where the probabilities of damage states ds_4 and ds_5 were notably above 0 for most perimeter columns but not for the internal columns. It should be noted that the damage state probabilities in Figure 9B were plotted only until reaching the collapse of the building. It can be seen that the collapse intensity for the characteristic ground motion was very different for the two buildings. The $im_{C,a}$ was about 3.5 g for the office building and about 0.29 g for the school building, but the values were not affected significantly by the structural models.

As in the case of the most vulnerable columns (Figure 9B), the IM-based damage state probabilities of other structural elements of the conventional MDOF model were found to be scattered around the probabilities determined for the corresponding IFB3 structural elements. Therefore, the probability $p_{DS,d,a,j}(im)$ determined for an IFB3 element was assigned in the loss analysis to all structural elements represented by that IFB3 element. In this way, the transformation from the rotations in the plastic hinges of the IFB3 elements to those of the actual structural elements was avoided. Such a transformation cannot be uniquely determined, as many different deformation shapes of the actual structure correspond to the same deformation shape in the IFB3 model. This may result in biased estimation of risk-based performance measures, but this bias is not significant for predominantly symmetrical buildings, as shown in Section 4.5. It should also be mentioned that a limitation of such an approach does not enable the direct capture of the variability in the damage state of the structural elements that are represented by the same IFB3 element. However, this limitation is inherent to all models that are based on the condensation of degrees of freedom.

On the other hand, the estimation of the IM-based damage state probabilities in the analysis utilizing the IFB3 model was more straightforward for the non-structural components. This is because the corresponding EDPs (drifts and accelerations) were uniquely determined based on the recordings from the structural analysis (see Section 4.2). The comparison of the IM-based damage state probabilities for characteristic ground motion is presented in Figure 10 for generic drift-sensitive components at the top of the bottom storey. It can be observed that there were only minor differences in the results obtained using the two models, regardless of the building. It is worth noting that the generic drift-sensitive components were considered to be located at the centre of mass (CM), which, however, is not the same as the centre of rigidity. Therefore, the inter-storey drifts at the location of these components were calculated based not only on the translation of the IFB3 columns but also on their torsional rotation.

4.4 | Loss analysis

The input for the loss analysis of both buildings, i.e. the loss functions $E(L_j^{'}|\ DS_j = ds_d)$, the quantities of components q_j and the costs of new components per unit $c_{new,j}$ are defined in the Appendix (Table 1 and Table 2). The costs $c_{new,j}$ were

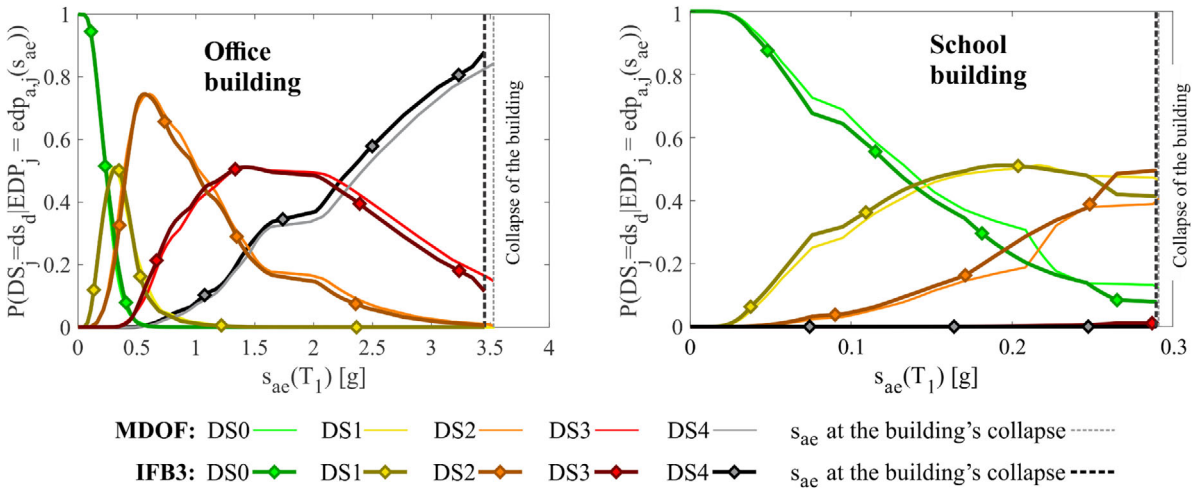

FIGURE 10 IM-based damage state probabilities of the generic drift-sensitive components located at the centre of mass at the top of the first storey of the office and school buildings. The probabilities were estimated using the IFB3 model and the conventional MDOF model and are conditional to the selected characteristic ground motion

estimated based on the average costs from Slovenian cost databases.[65,66] The loss functions for the structural components were estimated according to the costs of repair measures required to restore the damaged components. The repair measures were determined based on the FEMA PACT Tool,[62] while their costs were obtained from a Slovenian cost database.[65] For the non-structural components, most loss functions were obtained directly from the literature.[4,7,66] The exceptions were the stairs, the partition walls and the wooden attic of the school building. In the case of the stairs and partition walls, the loss functions were defined analogously to those determined for the structural components, that is by considering the repair measures as described in[62] and the costs provided in.[65] However, for the wooden attic, due to a lack of data, the normalised costs were determined based on the repair costs for timber structures provided in HAZUS.[5]

The construction costs of a new office building (L_{new}) were estimated by considering the mean construction costs per net floor area for mid-priced office and residential buildings in Slovenia (1100€ per m^2[66]). By considering the net floor area of the office building (389.4 m^2), the corresponding L_{new} was estimated at approximately 429,000€. For the school building, the construction cost was estimated at 1400€ per m^2 net floor area.[66] However, for the attic, the construction costs were reduced to 905€ per m^2 net floor area, which is a typical value for gyms located on the top storey.[66] The L_{new} for the school building, with a total net floor area of 2827 m^2, was thus estimated to be 3,582,000€.

The results of the loss analysis (Figures 11 and 12) are presented in terms of the losses conditional to the IM level. The losses presented in Figure 11 show the individual contributions of the structural, non-structural drift-sensitive and non-structural acceleration-sensitive components to the losses for non-collapse cases (Equation (10)). Therefore, they are presented only to the point of the building's collapse. It can be observed that the non-structural drift-sensitive components contributed most to the non-collapse losses of both buildings. It can also be observed that the differences between the results estimated using the IFB3 model and those estimated using the conventional MDOF model were negligible for the office building. On the other hand, some differences exist in the case of the school building. Namely, the IFB3 model slightly underestimated the losses in the structural elements at lower intensity levels, which was found to be related to the underestimation of damage in the beams. However, at higher intensity levels, the IFB3 model slightly overestimated the losses due to a sudden progression of damage compared to the conventional MDOF model, which was a consequence of the difference between the numbers of elements considered in the two models.

The losses presented in Figure 12 also considered the potential collapse of the building and the adjustments related to the restoration strategy. These were calculated as the average of the expected losses determined using Equation (11). In this case, too, the agreement between the losses obtained with both structural models was better for the office building. However, even for the school building, the results were not significantly different. The largest discrepancies can be observed in the median curve for intensities around 0.4 g. These discrepancies are a direct consequence of the differences in the collapse intensities, which were most pronounced in the range of collapse probabilities around 0.50 (see Figure 8). On the other hand, the matching is better for the 16^{th} and 84^{th} percentile as well as for the mean, which directly affects the expected annual loss (Section 4.5).

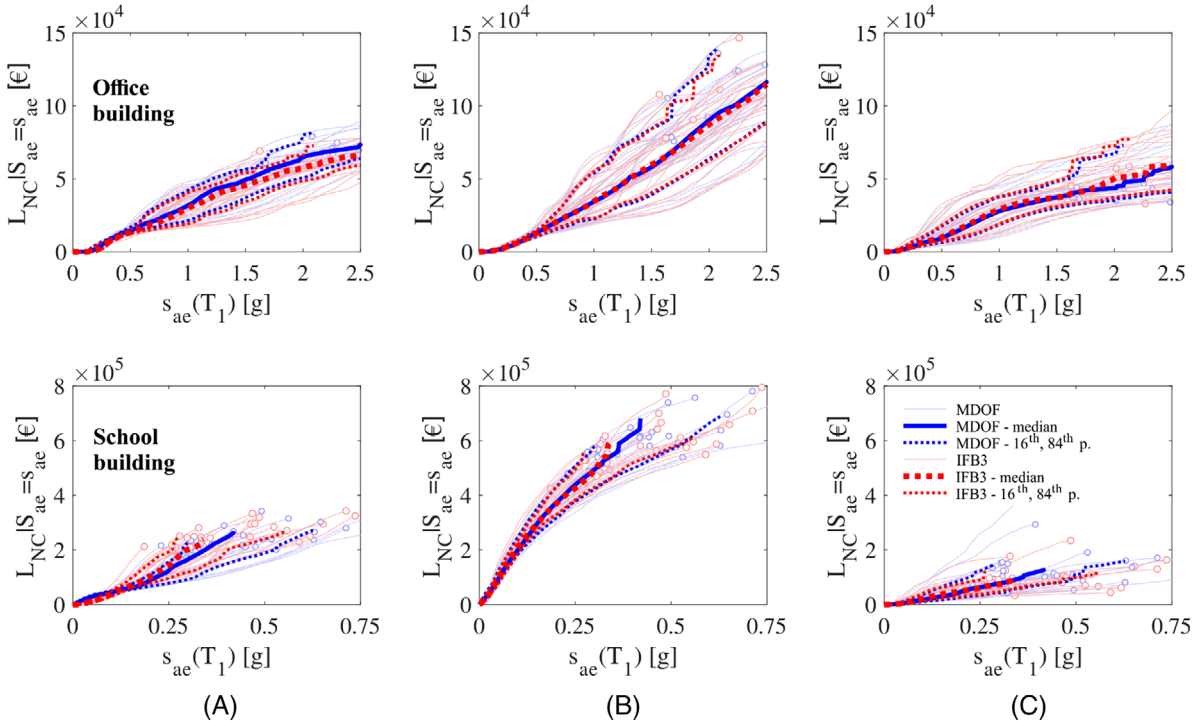

FIGURE 11 The losses for the non-collapse cases as a function of the IM level for the office and school buildings estimated with the IFB3 model and the conventional MDOF model: (A) The contribution of the structural components, (B) the contribution of the non-structural drift-sensitive components and (C) the contribution of the non-structural acceleration-sensitive components

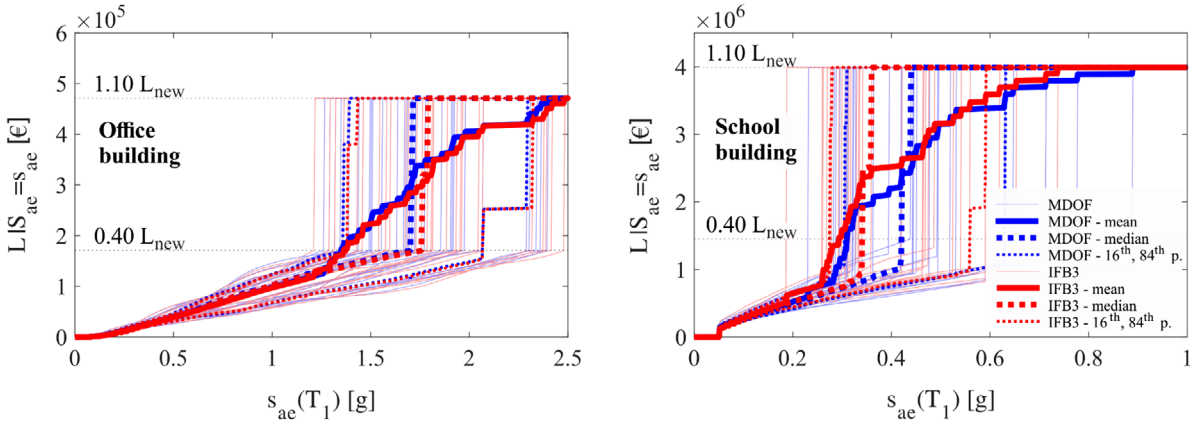

FIGURE 12 The total losses as a function of the IM level for each considered ground motion, determined as per Equation (11), and the corresponding mean, median, 16th percentile and 84th percentile. The losses are presented for the office and school buildings and were estimated with the IFB3 model and the conventional MDOF model

4.5 | Estimation of risk-based performance measures

Based on the hazard and loss analysis, risk-based performance measures introduced in Section 3.5 were estimated. The mean annual frequency of collapse $\lambda(C)$ for the office building was estimated at $2.59 \cdot 10^{-5}$ and $2.61 \cdot 10^{-5}$, respectively, for the analysis utilizing the IFB3 model and the conventional MDOF model. For the school building, which was not designed for earthquake resistance according to the modern codes, $\lambda(C)$ was significantly higher. It was estimated at $6.39 \cdot 10^{-4}$ and $5.26 \cdot 10^{-4}$ when employing the IFB3 model and the conventional MDOF model, respectively. Therefore, the IFB3 model overestimated the frequency of collapse of the office building and the school building by 1% and 21%,

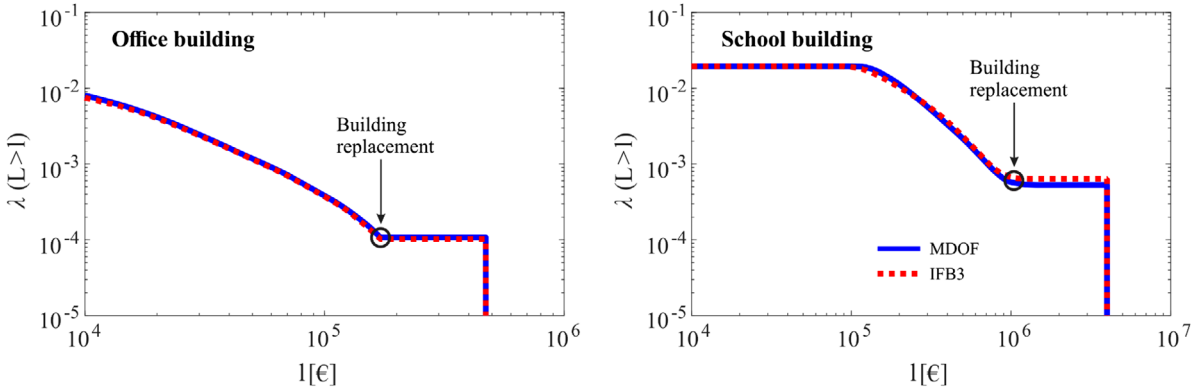

FIGURE 13 The probability of exceeding given loss based on the IFB3 and MDOF model for the office and school building

respectively, compared to the conventional MDOF model. These differences are not large, even for the school building, considering that the acceptable collapse risk for different reliability classes varies by a factor of about 10.[67]

The IFB3 model also provided a very similar estimation of the expected annual loss (EAL) compared to the conventional MDOF model. For the office building, EAL based on the IFB3 and conventional MDOF model amounted, respectively, to 331€ and 343€, which is about 0.08 % of the cost of a new building L_{new}. For the school building, EAL was estimated at 7565€ (0.21 % L_{new}) when using the IFB3 model, while a slightly lower EAL was estimated based on the conventional MDOF model (7308€, about 0.20 % L_{new}). Therefore, the difference in EAL estimated with the two structural models was 3–4 % for both analysed buildings.

Lastly, the IFB3 model and the conventional MDOF model also provided comparable results in terms of the mean annual frequency of the exceedance of a specified loss value, $\lambda(L > l)$ (Figure 13). It is interesting to note that the plateau of $\lambda(L > l)$ that appears in Figure 13 (left) for the office building is a consequence of the assumption that the stakeholders will most likely decide to replace the building if the total losses exceed 40% of L_{new}. The mean annual frequency of such an event (i.e. the ordinate of the plateau) was estimated at $1.0 \cdot 10^{-4}$, regardless of the structural model. Therefore, the replacement of the office building due to excessive damage is about four times more likely than its immediate collapse. However, in the case of the school building, the building's collapse took place before the losses exceeded the threshold for economically justified renovation for most considered ground motions. Therefore, the plateau of $\lambda(L > l)$ in this case reflects the effect of the building's collapse and its ordinate is practically the same as the mean annual frequency of collapse.

5 | CONCLUSION

The direct seismic loss estimation of predominantly plan-symmetrical frame buildings was investigated using a three-dimensional improved fish-bone model (i.e. the IFB3 model). For the analysed contemporary and older frame building, it was shown that the IFB3 model is capable of simulating EDPs and losses with similar accuracy to the conventional MDOF model. The difference in the expected annual loss estimated with the IFB3 model and the conventional MDOF model was only 3–4 % for both analysed buildings. The IFB3 model proved to be computationally efficient even though the loss estimation was based on the nonlinear response history analysis. The computational efficiency was reflected primarily in the case of the relatively complex school building. In this case, the computational time for the direct seismic loss estimation was reduced by a factor of 580.

Although it was demonstrated that the IFB3 model is computationally efficient and numerically robust and can provide loss estimates based on nonlinear response history analyses with sufficient accuracy, it has several limitations. New examples may help better understand the capabilities and limits of the presented IFB3 model in relation to different frame building typologies and loss estimation methodologies. They can also help further investigate if small differences in the EDPs always imply small differences in the estimated losses. Moreover, it had already been determined that fish-bone models are unsuitable for seismic analysis of frame buildings with a large height-to-length ratio. This limitation also applies to the IFB3 model. Furthermore, the IFB3 model cannot directly simulate the damage in individual structural components, as they are condensed at the storey level into IFB3 elements. The latter limitation may impact loss estimation in the case of plan-asymmetrical buildings. Additional research is thus needed to develop simplified models capable of simulating

seismic response and losses in more complex structural systems. Such models will become attractive for the loss estimation of building portfolios, which is the ultimate goal of developing simplified structural models, where time efficiency and computational robustness are of significant importance.

ACKNOWLEDGEMENTS

The research presented in this paper is based on work financed by the Slovenian Research Agency as part of the research program Earthquake Engineering (P2-0185). This support is gratefully acknowledged.

DATA AVAILABILITY STATEMENT

The data that support the findings of this study are available from the corresponding author upon reasonable request.

ORCID

Anže Babič https://orcid.org/0000-0002-4183-5675
Matjaž Dolšek https://orcid.org/0000-0003-3564-5135

REFERENCES

1. Porter KA, Kiremidjian AS. *Assembly-Based Vulnerability of Buildings and its Uses in Seismic Performance Evaluation and Risk Management Decision-Making*. John A. Blume Earthquake Engineering Research Center; 2001. Report 133.
2. Aslani H, Miranda E. *Probabilistic earthquake estimation and loss disaggregation in buildings*. Stanford University, The John A. Blume Earthquake Engineering Center Department of Civil and Environmental Engineering; 2005. Report no. 157.
3. Mitrani-Reiser J, Beck J. *An Ounce of Prevention: Probabilistic Loss Estimation for Performance-based Earthquake Engineering*. Department of Civil Engineering and Applied Mechanics, California Institute of Technology; 2007.
4. Bradley BA. *Structure-specific probabilistic seismic risk assessment. Doctoral dissertation. Department of Civil and Natural Resources Engineering*. University of Canterbury; 2009.
5. FEMA. *HAZUS MH 2.1, Multi-Hazard Loss Assessment Methodology*. Federal Emergency Management Agency; 2015.
6. ATC. *FEMA P-58-1 – Seismic performance assessment of buildings, Volume 1 – Methodology*. FEMA; 2018.
7. Snoj J, Dolšek M. Pushover-based seismic risk assessment and loss estimation of masonry buildings. *Earth Eng Struct Dyn*. 2020;49:567-588.
8. Sousa L, Silva V, Marques M, Crowley H. On the treatment of uncertainties in the development of fragility functions for earthquake loss estimation of building portfolios. *Earth Eng Struct Dyn*. 2016;45:1955-1976.
9. Ibarra LF, Krawinkler H, Global Collapse of Frame Structures under Seismic Excitations, John A. Blume Earthquake Engineering Center, Stanford University, CA; 2005; Report No. 152.
10. Haselton CB, Goulet CA, Mitrani-Reiser J, et al. *An Assessment to Benchmark the Seismic Performance of a Code-Conforming Reinforced Concrete Moment-Frame Building*. PEER Center; 2008. PEER Report 2007/12.
11. Jamšek A, Dolšek M. Seismic analysis of older and contemporary reinforced concrete frames with the improved fish-bone model. *Eng Struct*. 2020:212.
12. Cardone D, Sullivan T, Gesualdi G, Perrone G. Simplified estimation of the expected annual loss of reinforced concrete buildings. *Earth Eng Struct Dyn*. 2017;46:2009-2032.
13. Martins L, Silva V, Marques M, Crowley H, Delgado R. Development and assessment of damage-to-loss models for moment-frame reinforced concrete buildings. *Earth Eng Struct Dyn*. 2016;45:797-817.
14. FEMA P695. *Quantification of Building Seismic Performance Factors*. Federal Emergency Management Agency, 2009.
15. Gogus A, Wallace JW. Seismic Safety Evaluation of Reinforced Concrete Walls through FEMA P695 Methodology. *J Struct Eng*. 2015;10.
16. Vamvatsikos D, Cornell CA. Direct estimation of the seismic demand and capacity of oscillators with multi-linear static pushovers IDA. *Earth Eng Struct Dyn*. 2006;35(9):1097-1117.
17. Ogawa K, Kamura H, Inoue K. Modeling of the moment resistant frame to fishbone-shaped frame for the response analysis. *J Str Constr Eng*. 1999;521:119-126.
18. Nakashima M, Ogawa K, Inoue K. 2002. Generic frame model for simulation of earthquake responses of steel moment frames. *Earth Eng Struct Dyn*. 2002;31:671-692.
19. Luco N, Mori Y, Funahashi Y, Cornell CA, Nakashima M. Evaluation of predictors of non-linear seismic demands using 'fishbone' models of SMRF buildings. *Earth Eng Struct Dyn*. 2003;32:2267-2288.
20. Khaloo AR, Khosravi H. Modified fishbone model: a simplified MDOF model for simulation of seismic responses of moment resisting frames. *Soil Dyn Earth Eng*. 2013;55:195-210.
21. Khaloo AR, Khosravi H, Jamnani HH. Nonlinear Interstory Drift Contours for Idealized Forward Directivity Pulses using "Modified Fish-Bone" Models. *Adv Struct Eng*. 2015;18(5):603-627.
22. Araki Y, Ohno M, Mukai I, Hashimoto N. Consistent DOF reduction of tall steel frames. *Earth Eng Struct Dyn*. 2017;46:1581-1597.
23. Haghighat A, Sharifi A. Evaluation of Modified Fish-Bone Model for Estimating Seismic Demands of Irregular MRF Structures. *Period Polyt Civ Eng;*. 2018:1-12.

24. Zhe Q, Ting G, Qiqi L, Tao W. Evaluation of the fishbone model in simulating the seismic response of multistorey reinforced concrete moment-resisting frames. *Earthq Eng Eng Vibr*. 2019;18(2):315-330.
25. Soleimani R, Khosravi H, Hamidi H. Substitute Frame and adapted Fish-Bone model: two simplified frames representative of RC moment resisting frames. *Eng Struct*. 2019;185:68-89.
26. Soleimani R, Hamidi H. General Substitute Frame Model (GSF) for efficient estimation of seismic demands of steel and RC moment frames. *Eng Struct*. 2021;246(1):113031.
27. Jamšek A, Dolšek M. The Reduced-Degree-of-Freedom Model for Seismic Analysis of Predominantly Plan-Symmetric Reinforced Concrete Wall-Frame Building. *Build*. 2021;11(8):372.
28. Jamšek A. *Seismic stress test with incomplete building data (in Slovenian)*. University of Ljubljana, Faculty of Civil and Geodetic Engineering; 2020. PhD Dissertaion.
29. CEN. *Eurocode 2: Design of concrete structures – Part 1-1: General rules and rules for buildings*. European Committee for Standardization, 2004.
30. CEN. *Eurocode 8: Design of structures for earthquake resistance – Part 1: General rules, seismic actions and rules for buildings*. European Committee for Standardization, 2004.
31. Dolšek M. Development of computing environment for the seismic performance assessment of reinforced concrete frames by using simplified nonlinear models. *Bull Earthq Eng*. 2010;8:1309-1329.
32. Paulay T, Priestley MJN. *Seismic design of reinforced concrete and masonry structures*. John Wiley and Sons; 1992.
33. MathWorks. MATLAB the Language of Technical Computing, http://www.mathworks.com/; 2020.
34. PEER. *Open System for Earthquake Engineering Simulation (OpenSees)*. Pacific Earthquake Engineering Research Center. 2007.
35. Altoontash A. *Simulation and damage models for performance assessment of reinforced concrete beam-column joints*. The Department of the Civil and Environmental Engineering, Stanford University; 2004. Doctoral Dissertation.
36. De Risi MT, Ricci P, Verderame GM. Modelling exterior unreinforced beam-column joints in seismic analysis of non-ductile RC frames. *Earth Eng Struct Dyn*. 2017;46:899-923.
37. O'Reilly GJ, Sullivan TJ. Modeling Techniques for the Seismic Assessment of the Existing Italian RC Frame Structures. *J Earthq Eng*. 2019;23(8):1262-1296.
38. Vamvatsikos D, Cornell CA. Incremental Dynamic Analysis. *Earth Eng Struct Dyn*. 2002;31(3):491-514.
39. Baker JW. Efficient Analytical Fragility Function Fitting Using Dynamic Structural Analysis. *Earthq Spec*. 2015;31(1):579-599.
40. Uradni list RS. Buildings reconstruction program following the earthquake in Posočje on July 12 2004 for the years 2011 and 2012. Official Journal Government of the Republic of Slovenia, No. 34008-/3/2011/5. (in Slovenian); 2011.
41. Rosti A, Rota M, Penna A. Damage classification and derivation of damage probability matrices from L'Aquila (2009) post-earthquake survey data. *Bull Earthq Eng*. 2018;16(1):3687-3720.
42. Fardis MN. *Experimental and numerical investigations on the seismic reponse of RC infilled frames and recommendations for code provisions*. LNEC; 1996. ECOEST/PREC8, Rep. No. 6.
43. Negro P, Colombo A. Irregularities induced by non-structural masonry panels in framed buildings. *Eng Struct*. 1996;19(7):576-585.
44. Graphisoft. ArchiCAD 22. http://www.graphisoft.com/archicad/; 2019.
45. Uradni list FNRJ. *Privremeni tehnički propisi za beton i armirani beton PTP-3*. Federativna Narodna Republika Jugoslavija; 1947.
46. Uradni list SRS. Odredba o dimenzioniranju in izvedbi gradbenih objektov v potresnih območjih. Uradni list SRS, št. 18/63; 1963.
47. CEN. *Eurocode 8: Design of structures for earthquake resistance – Part 2: Bridges*. European Committee for Standardization, 2005.
48. Lapajne J, Motnikar BŠ, Zupančič P. Probabilistic Seismic Hazard Assessment Methodology for Distributed Seismicity. *Bull Seism Soc Am*. 2003;93(6):2502-2515.
49. Jayaram N, Lin T, Baker JW, A Computationally Efficient Ground-Motion Selection Algorithm for Matching a Target Response Spectrum Mean and Variance. Earthq Spec. 2011;27(3):797-815.
50. Baker JW. Conditional mean spectrum: tool for ground-motion selection. *J Struct Eng*. 2011;137(3):322-331.
51. Chiou B, Darragh R, Gregor N, Silva W. NGA project strong-motion database. *Earthq Spec*. 2008;24(1):23-44.
52. Akkar S, Sandikkaya MA, Şenyurt M, et al. Reference database for seismic ground-motion in Europe (RESORCE). *Bull Earth Eng*. 2014;12:311-339.
53. Zacharenaki A, Fragiadakis M, Assimak D, Papadrakakis M. Bias assessment in incremental dynamic analysis due to record scaling. *Soil Dyn Earth Eng*. 2014;67:158-168.
54. Chopra AK, Goel RK. Evaluation of NSP to estimate seismic deformation: sDF systems. *J Struct Eng*. 2000;126(4):482-490.
55. Fajfar P. Capacity spectrum method based on inelastic demand spectra. *Earthq Eng Struct Dyn*. 1999;28:979-993.
56. Miranda E. Inelastic displacement ratios for structures on firm sites. *J Struct Eng*. 2000;126(10):1150-1159.
57. Vukobratović V, Fajfar P. Code-oriented floor acceleration spectra for building structures. *Bull Earthq Eng*. 2017;15:3013-3026.
58. Jalayer F, Ebrahimian H, Miano A, Manfredi G, Sezen H. Analytical fragility assessment using unscaled ground motion records. *Earthq Eng Struct Dyn*. 2017;46:2639-2663.
59. Shinozuka M, Feng MQ, LeeJ NaganumaT. Statistical Analysis of Fragility Curves. *J Eng Mech*. 2000;126:1224-1231.
60. Straub D, Der Kiureghian A. Improved seismic fragility modeling from empirical data. *Struct Saf*. 2008;30:320-336.
61. Cardone D, Perrone G. Developing fragility curves and loss functions for masonry infill walls. *Earthq Struct*. 2015;9(1):257-279.
62. ATC. *FEMA P-58-2 – Seismic performance assessment of buildings, Volume 2 – Implementation guide*. FEMA; 2018.
63. Panagiotakos TB, Fardis M. Deformations of reinforced concrete at yielding and ultimate. *ACI Struct J*. 2001;98(2):135-147.

64. Peruš I, Poljanšek K, Fajfar P. Flexural deformation capacity of rectangular RC columns determined by the CAE method. *Earthq Eng Struct Dyn*. 2006;30:1453-1470.
65. Cening. Building construction cost book. Inženiring biro Marinko d.o.o (in Slovenian); 2017.
66. PEG. Civil Engineering online portal - PEG. http://www.peg-online.net/ (in Slovenian); 2020.
67. CEN. *Eurocode 0: Basis of Structural Design*. European Committee for Standardization, 2002.

How to cite this article: Jamšek A, Babič A, Dolšek M. Direct seismic loss estimation of predominantly plan-symmetrical frame buildings using simplified nonlinear models. *Earthquake Engng Struct Dyn*. 2022;51:3526–3551. https://doi.org/10.1002/eqe.3734

APPENDIX

TABLE 1 Parameters of fragility and loss functions component j ($\widetilde{EDP}_{ds,j}$ – the median EDP causing the damage state, $\beta_{ds,j}$ – the corresponding logarithmic standard deviation, $\overline{c_{new,j}}$ – average cost of a new component, $E'(L_j|DS = ds)$– normalised expected losses due to a damage state ds) and the units, units per componentq_j and quantity of component for the whole building Σq_j) of the office building

		Units and quantities			Fragility functions			Loss functions		
Component	**Description**	**Unit**	**Units per component (q_j)**	**Quantity Σq_j (whole building)**	**ds_j**	**EDP**	**$\widetilde{EDP}_{ds,j}$**	**$\beta_{ds,j}$**	**$\overline{c_{new,j}}$**	**$E'(L_j \|DS = ds)$**
Column	Reinforced concrete column	1 column	1	36 columns	$ds1$	$\Theta[rad]$	$\Theta_{p=1}$	0.36	820€/unit	0.17
					$ds2$		$(\Theta_{p=1} + \Theta_{p=2})/2$	0.36		0.83
					$ds3$		$\Theta_{p=2}$	0.40		0.95
					$ds4$		$\Theta_{p=3}$	0.40		1.10
Beam	Reinforced concrete beam with effective slab widths	1 beam	1	48 beams	$ds1$	$\Theta[rad]$	$\Theta_{p=1}$	0.36	1450€/unit	0.18
					$ds2$		$(\Theta_{p=1} + \Theta_{p=2})/2$	0.36		0.74
					$ds3$		$\Theta_{p=2}$	0.60		0.93
					$ds4$		$\Theta_{p=3}$	0.60		1.10
Partition wall	Gypsum – board partitions	1 m^2 of wall	Varies (15.5 m^2 on average)	310 m^2 (20 components)	$ds1$	IDR [%]	0.40	0.56	58€/unit	0.10
					$ds2$		0.78	0.27		0.60
					$ds3$		1.10	0.25		1.20
Exterior glazing	Exterior glazing - horizontal wall system	1 m^2 of glazing	2.7	432 m^2 (160 components)	$ds1$	IDR [%]	4.00	0.36	311€/unit	1.00
					$ds2$		4.60	0.33		1.00
Chimney	Masonry chimney	1 m of chimney	14	14 m (1 component)	$ds1$	PFA [g]	0.35	0.60	150€/unit	0.87
					$ds2$		0.50	0.60		1.20
Roof	Clay tile roof, tiles secured	1 m^2 of roof	108.2	108.2 m^2 (1 component)	$ds1$	PFA [g]	1.40	0.30	70€/unit	0.44
					$ds2$		1.70	0.30		1.00
Suspended ceiling	Ceiling Systems Suspended acoustical type	1 m^2 of suspended ceiling	Varies (90.8 m^2 on average)	363.2 m^2 (4 components)	$ds1$	PFA [g]	0.27	0.40	22.5€/unit	0.12
					$ds2$		0.65	0.50		0.36
					$ds3$		1.28	0.55		1.20

(Continues)

TABLE 1 (Continued)

		Units and quantities			Fragility functions			Loss functions		
Component	**Description**	**Unit**	**Units per component (q_j)**	**Quantity Σq_j (whole building)**	ds_j	EDP	$\widehat{EDP}_{ds,j}$	$\beta_{ds,j}$	$\overline{c_{new,j}}$	$E'(L_j \mid DS = ds)$
Stair	Reinforced concrete, cast in place	1 staircase	1	4 staircases	$ds1$	IDR [%]	0.50	0.6	1780€/unit	0.22
					$ds2$		1.70	0.6		0.58
					$ds3$		2.80	0.45		1.00
Door	Interior glass door	1 door	1	20 doors	$ds1$	IDR [%]	3.03	0.50	450€/unit	0.10
					$ds2$		4.13	0.50		0.60
					$ds3$		5.10	0.50		1.20
Elevator	Elevator with semi-automatic glass door	1 elevator	1	1 elevator	$ds1$	PGA [g]	0.41	0.28	18,000€/unit	1.00
Generic drift sensitive	Vertical piping, bath tubs, fire hose cabinet	All generic drift-sensitive components per storey	1	Components in all 4 storeys (4 components)	$ds1$	IDR [%]	0.40	0.50	13,000€/unit	0.025
					$ds2$		0.80	0.50		0.10
					$ds3$		2.50	0.50		0.60
					$ds4$		5.00	0.50		1.20
Generic acceleration sensitive	Plumbing, toilets, HVAC, heating, cooling	All generic acceleration-sensitive components per storey	1	Components in all 4 storeys (4 components)	$ds1$	PFA[g]	0.25	0.60	13,000€/unit	0.020
					$ds2$		0.50	0.60		0.12
					$ds3$		1.00	0.60		0.36
					$ds4$		2.00	0.60		1.20

TABLE 2 Parameters of fragility and loss functions component j ($\widetilde{EDP_{ds,j}}$ – the median EDP causing the damage state, $\beta_{ds,j}$ – the corresponding logarithmic standard deviation, $\overline{c_{new,j}}$ – average cost of a new component, $E'(L_j|DS = ds)$– normalized expected losses due to a damage state ds) and the units, units per componentq_j and quantity of component for the whole building Σq_j) of the school building

		Units and quantities			Fragility functions			Loss functions		
Component	**Description**	**Unit**	**Units per component (q_j)**	**Quantity Σq_j (whole building)**	ds_j	EDP	$\widetilde{EDP_{ds,j}}$	$\beta_{ds,j}$	$\overline{c_{new,j}}$	$E'(L_j \|DS = ds)$
Column	Reinforced concrete column	1 column	1	320 columns	$ds1$	$\Theta[rad]$	$\Theta_{p=1}$	0.36	790€/unit	0.19
					$ds2$		$(\Theta_{p=1} + \Theta_{p=2})/2$	0.36		0.81
					$ds3$		$\Theta_{p=2}$	0.40		0.93
					$ds4$		$\Theta_{p=3}$	0.40		1.10
Beam	Reinforced concrete beam with effective slab widths	1 beam	1	472 beams	$ds1$	$\Theta[rad]$	$\Theta_{p=1}$	0.36	930€/unit	0.18
					$ds2$		$(\Theta_{p=1} + \Theta_{p=2})/2$	0.36		0.77
					$ds3$		$\Theta_{p=2}$	0.60		0.92
					$ds4$		$\Theta_{p=3}$	0.60		1.10
Partition wall	Masonry partitions (*without openings/ **with window openings/ ***with door openings)	1 m^2 of wall	Varies (49.9 m^2 on average)	64 units (3196 m^2)	$ds1$	IDR [%]	*0.15/ **0.10/ ***0.075	0.45	3898€/unit (78€/m^2)	0.30
					$ds2$		*0.40/ **0.30/ ***0.20	0.41		0.64
					$ds3$		*1.00/ **0.74/ ***0.50	0.26		1.00
					$ds4$		1.75	0.18		1.00
Window	Exterior window	1 window	1	196 units	$ds1$	IDR [%]	1.60	0.29	870€/unit (311€/m^2)	0.10
					$ds2$		3.20	0.29		0.60
					$ds3$		3.60	0.27		1.20
Chimney	Masonry chimney	1 m of chimney	14	1 unit	$ds1$	PFA [g]	0.35	0.60	7560€/unit (540€/m)	0.87
					$ds2$		0.50	0.60		1.20
Roof	Clay tile roof, unsecured tiles	1 m^2 of roof	983	983 m^2 (1 component)	$ds1$	PFA [g]	0.40	0.30	70€/m^2	0.53
					$ds2$		0.50	0.30		1.00

(Continues)

TABLE 2 (Continued)

		Units and quantities			Fragility functions			Loss functions		
Component	Description	Unit	Units per component (q_j)	Quantity Σq_j (whole building)	ds_j	EDP	$\widetilde{EDP}_{ds,j}$	$\beta_{ds,j}$	$\overline{c_{new,j}}$	$E'(L_j \mid DS = ds)$
Wooden attic frame structure	Wooden framing and gym equipment in the attic	1 unit of wooden attic with framing and equipment	1	1 unit	$ds1$	PFA [g]	0.25	0.64	395,000€/unit	0.02
					$ds2$		0.35	0.64		0.10
					$ds3$		0.64	0.64		0.44
					$ds4$		1.13	0.64		1.00
Stair	Reinforced concrete, cast in place	1 staircase	1	5 units	$ds1$	IDR [%]	0.50	0.60	4210€/unit	0.27
					$ds2$		1.70	0.60		0.64
					$ds3$		2.80	0.45		1.00
Door	Interior glass door with skylight	1 unit	1	60 units	$ds1$	IDR [%]	3.03	0.50	1050€/unit (205€/m^2)	0.10
					$ds2$		4.13	0.50		0.60
					$ds3$		5.10	0.50		1.20
Generic drift sensitive	Vertical piping, bath tubs, fire hose cabinet	All generic drift sensitive components per storey	1	4 storeys	$ds1$	IDR [%]	0.40	0.50	144,000€/storey	0.025
					$ds2$		0.80	0.50		0.10
					$ds3$		2.50	0.50		0.60
					$ds4$		5.00	0.50		1.20
Generic acceleration sensitive	Plumbing, toilets, HVAC, heating, cooling	All generic acceleration sensitive components per storey	1	4 storeys	$ds1$	PFA [g]	0.25	0.60	144,000€/storey	0.020
					$ds2$		0.50	0.60		0.12
					$ds3$		1.00	0.60		0.36
					$ds4$		2.00	0.60		1.20